University of Zurich[UZH]

Zurich Open Repository and Archive
University of Zurich
University Library
Strickhofstrasse 39
CH-8057 Zurich
www.zora.uzh.ch

Year: 2017

Terrestrial laser scanning for forest inventories—tree diameter distribution and scanner location impact on occlusion

Abegg, Meinrad ; Kükenbrink, Daniel ; Zell, Jürgen ; Schaepman, Michael E ; Morsdorf, Felix

Abstract: The rapid development of portable terrestrial laser scanning (TLS) devices in recent years has led to increased attention to their applicability for forest inventories, especially where direct measurements are very expensive or nearly impossible. However, in terms of precision and reproducibility, there are still some pending questions. In this study, we investigate the influence of stand parameters on the TLS-related visibility in forest plots. We derived 2740 stand parameters from Swiss national forest inventory sample plots. Based on these parameters, we defined virtual scenes of the forest plots with the software "Blender". Using Blender's ray-tracing features, we assessed the 3D coverage in a cubic space and 2D visibility properties for each of the virtual plots with different scanner placement schemes. We provide a formula to calculate the maximum number of possible hits for any object size at any distance from a scanner with any resolution. Additionally, we show that the Weibull scale parameter describing a stand, in addition to the number of trees and the mean diameter of the dominant 100 trees per hectare, has a significant and relevant influence on the visibility of the sample plot. Furthermore, we show the effectiveness and the efficiency of 40 scanner location patterns. These experiments demonstrate that intuitively distributing scanner locations evenly within the sample plot, with similar distances between locations and from the edge of the sample plot, provides the best overall visibility of the stand.

DOI: https://doi.org/10.3390/f8060184

Posted at the Zurich Open Repository and Archive, University of Zurich
ZORA URL: https://doi.org/10.5167/uzh-138638
Journal Article
Published Version

The following work is licensed under a Creative Commons: Attribution 4.0 International (CC BY 4.0) License.

Originally published at:
Abegg, Meinrad; Kükenbrink, Daniel; Zell, Jürgen; Schaepman, Michael E; Morsdorf, Felix (2017). Terrestrial laser scanning for forest inventories—tree diameter distribution and scanner location impact on occlusion. Forests, 8(6):184.
DOI: https://doi.org/10.3390/f8060184

forests

MDPI

Article

Terrestrial Laser Scanning for Forest Inventories—Tree Diameter Distribution and Scanner Location Impact on Occlusion

Meinrad Abegg [1,2,*], Daniel Kükenbrink [2], Jürgen Zell [1], Michael E. Schaepman [2] and Felix Morsdorf [2]

[1] Forest Resources and Management, WSL Swiss Federal Institute for Forest, Snow and Landscape Research WSL, Zürcherstrasse 111, CH-8903 Birmensdorf, Switzerland; juergen.zell@wsl.ch

[2] Remote Sensing Laboratories, Department of Geography, University of Zurich, Winterthurerstr 190, CH-8057 Zürich, Switzerland; daniel.kuekenbrink@geo.uzh.ch (D.K.); michael.schaepman@geo.uzh.ch (M.E.S.); felix.morsdorf@geo.uzh.ch (F.M.)

* Correspondence: meinrad.abegg@wsl.ch; Tel.: +41-44-739-2412

Academic Editor: Timothy A. Martin
Received: 31 March 2017; Accepted: 20 May 2017; Published: 26 May 2017

Abstract: The rapid development of portable terrestrial laser scanning (TLS) devices in recent years has led to increased attention to their applicability for forest inventories, especially where direct measurements are very expensive or nearly impossible. However, in terms of precision and reproducibility, there are still some pending questions. In this study, we investigate the influence of stand parameters on the TLS-related visibility in forest plots. We derived 2740 stand parameters from Swiss national forest inventory sample plots. Based on these parameters, we defined virtual scenes of the forest plots with the software "Blender". Using Blender's ray-tracing features, we assessed the 3D coverage in a cubic space and 2D visibility properties for each of the virtual plots with different scanner placement schemes. We provide a formula to calculate the maximum number of possible hits for any object size at any distance from a scanner with any resolution. Additionally, we show that the Weibull scale parameter describing a stand, in addition to the number of trees and the mean diameter of the dominant 100 trees per hectare, has a significant and relevant influence on the visibility of the sample plot. Furthermore, we show the effectiveness and the efficiency of 40 scanner location patterns. These experiments demonstrate that intuitively distributing scanner locations evenly within the sample plot, with similar distances between locations and from the edge of the sample plot, provides the best overall visibility of the stand.

Keywords: terrestrial laser scanning; forest inventory; occlusion; stem diameter distribution

1. Introduction

National Forest Inventories (NFI) deliver information on the forest area, the amount and change of forest resources, the development of the biotope forest in general, the carbon balance of a country [1–3] and other ecosystem services [4]. In the Swiss NFI, data collection is based on aerial photo interpretation, forest service interviews and field measurements [5]. Field measurements provide the largest and most important collection of data for a NFI. On a national level, they comprise measurements of several thousand sample plots, each of which has to be visited by a field team [6]. Field measurements consist of two methods: actual measurements and expert assessments. If possible, measurements are applied to determine forest features. However, certain forest features are nearly impossible to measure on standing trees or can only be measured at a very high cost with traditional

tools. Examples of such features are tree volume, forest structure, crown size and shape, gap size and light availability at certain heights above ground. The medium-term objective of the Swiss NFI is to replace or enhance expert assessments with actual measurements where possible. The development of portable terrestrial LiDAR devices in recent years and increased computing power lead to the question of whether these devices can be used for forest inventories to enhance the efficiency and improve data quality.

Given the high costs of terrestrial laser scanning systems (TLS) and the time-consuming measurement process, the added value of TLS for forest inventories needs to be clearly demonstrated in terms of efficiency, robustness and precision. One evaluation method is to simulate a virtual forest and a virtual instrument, as described by several authors [7–10]. The advantage of the simulation approach is that many configurations can be tested with only little expense for additional samples. Still, the simulation environment is merely an abstraction of reality and, consequently, the representativeness of the virtual scene has to be considered carefully. Several factors, such as scanning resolution, the LiDAR technology applied, and weather conditions, influence the quality of the laser scans in terms of completeness and accuracy. However, as mentioned by various authors (e.g., [11–13]), occlusion is one of the key factors that limits the potential of TLS. Occlusion is caused by objects shadowing each other, so that parts of the objects of interest are not visible to the TLS device. The effect of occlusion is usually mitigated by combining TLS scans from different locations [14]. In the literature, various scanner location combination patterns are described (e.g., [11,15–17]). Trochta et al. [12] compare the quality of multiple scans in natural beech forests. Van der Zande et al. [9] evaluate three different scanner position combinations, each in three different types of stands. However, for the possible applications of TLS in forest inventory, the methods need to have a proven high performance in a larger range of forest stand conditions. The decision maker of a forest inventory needs a fundamental understanding of the influencing factors regarding the quality of the point clouds generated by TLS and possible constraints on operational applications. The analysis of visibility can contribute to quantifying the expected quality of TLS acquisitions in terms of completeness.

The goal of this study is to highlight both the potential and the limitations of TLS in terms of expected TLS points per object and to explain the influence of the stand and the scanner placement on the quality of the scans in terms of completeness. We therefore use simulations in order to explore the widest possible range of stand and scanner placement characteristics. Our objectives are:

(i) To demonstrate the relationships between angular resolution of the scanner, object size, distance to the scanner and the possible sampling frequency (scanner point density) on an object with TLS in a 3D space. This should help determine the minimal object size detectable by TLS.
(ii) To show the connection between the visibility of a sample plot and its stand describing parameters, such as diameter distribution, stem number and dominant diameter. This experiment improves the understanding of how the stand properties influence the scan quality. We hypothesize that there is a very strong link between the stand parameters and the visibility.
(iii) To demonstrate the influence of the scanning location within a sample plot on the visibility.
(iv) To understand the mechanism behind occlusion and to determine the most suitable scanner location patterns for TLS acquisitions in forests.

2. Materials and Methods

2.1. The NFI Framework, Data and Tools

2.1.1. Sample Plot

Depending on the target variable, different plot sizes are used in the Swiss NFI. The radii of the six sample plots for the tree measurement of the different diameter classes range from 0.9 m to 12.62 m (0.9 m, 1.5 m, 2.5 m, 4 m, 7.98 m, 12.62 m). The largest sample plot, a square area of 50 × 50 m termed the "interpretation area", is used to assess stand level parameters, such as stand structure and occurrence

of important elements in the stand, such as snags or coverage of regeneration [18]. For the evaluations of TLS applications, we chose to evaluate this largest area because all the sample plots of the Swiss NFI are contained within this area. For the evaluation, we defined the sample plot into a 2-dimensional cartesian coordinate system. The centre of the sample plot is located at the x–y-coordinates (0, 0).

2.1.2. NFI Data

NFI data are commonly collected on sample plots arranged in a regular grid over an area of interest. This allows for a statistical inference of population values, such as stem number, for the investigated area [19]. Since the year 2009, the Swiss NFI has conducted its field measurements on nine equally sized grids, which are placed so that all the grids combined constitute one regular grid with a mesh size of approximately 1.41 km ($\sqrt{2}$). This always allows a representative evaluation of either single or combined grids.

At each grid intersection point, the trees are recorded on different circular plots depending on their size as mentioned earlier (Size classes: 0.1 m–0.39 m height, 0.4–1.29 m height, 0.1–3.9 cm DBH, 4–11.9 cm DBH, 12–35.9 cm DBH, $\geq$36 cm DBH). Nevertheless, the methods applied are the same, allowing all the measured trees of any given diameter at breast height (DBH) to be combined. Since every tree of any diameter contributes to occlusion, we included all trees reaching 1.3 m in height for our evaluation. We used the combined datasets of all the trees per grid intersection point, respecting their statistical selection probability, to derive stand describing parameters.

The Weibull distribution is a common choice for describing the density of diameters in a stand [20]. It is a left-truncated distribution and can handle a wide spectrum of stand situations. The Weibull distribution consists of three parameters, a shape (W_{shape}), a scale (W_{scale}) and an offset that describes the smallest diameter. The offset was set to 0.5 cm as a fixed parameter because this is the smallest diameter measured at breast height. W_{shape} and W_{scale} were estimated by maximising the likelihood function of the Weibull distribution, given the observations. Since this estimation is subject to a stochastic process, we excluded extreme outliers which we could identify with commonly used NFI parameters. We excluded the simulated samples that exceeded double the maximal determined D_{dom} in a Swiss NFI field campaign (185 cm) and all the samples that have one simulated diameter that exceeds three times the maximal measured diameter in the Swiss NFI of 207 cm. With this variability, we covered all the possible stand parameters that are likely to occur in the Swiss forests and included some extreme values as well.

2.1.3. Blender

Blender [21] is an open-source 3D content creation suite. For this publication, we used version 2.74. Blender can be fully controlled using the programming language python. It allows the user to create 3D objects and define their light interaction properties. These features are normally used to render photorealistic images or animated movies. Blender provides a large toolbox to define, manipulate and store 3D objects.

We used Blender and the stand parameters to set up cylinders as a proxy for trees for a visibility assessment (see Figure 1). The Weibull parameters W_{shape} and W_{scale} defined the shape of the diameter distribution. N_{tree} on the other hand, defined the number of cylinders to be set up. A random number generator for Weibull distributions in the python library "numpy" provided the diameters of the cylinders. The locations of the cylinders were calculated by a random uniform number generator, which leads to Poisson-distributed cylinders on the sample plot. No cylinder was allowed to overlap the scanner positions or another cylinder, and any overlapping cylinders were relocated to a new random position within the sample plot. The cylinders were initially defined as a Bézier curve with a certain diameter (bevel) and then converted to a mesh. A mesh is defined in Blender as a number of points (vertices) that are connected with lines (edges) and polygons (faces). The time needed for the definition of new cylinders increases exponentially, so we sourced out the definition of new cylinders when N_{tree} exceeded 4000. For this step, we used a Blender feature called particle systems.

With particle systems, a single object can be multiplied and randomly placed, without using much computing power, by defining the number and the random locations with a mathematical equation. We used particle systems to randomly place the smallest trees (cylinders), which are the single reason for higher N_{tree} values. To avoid overlapping with the scanner location, we spared an area of 0.04 m^2 around the scanner positions. To account for particle system cylinders located within larger cylinders, which were not defined by a particle system, we increased the number of particle cylinders using the ratio of the basal area of the larger cylinders to the sample plot size.

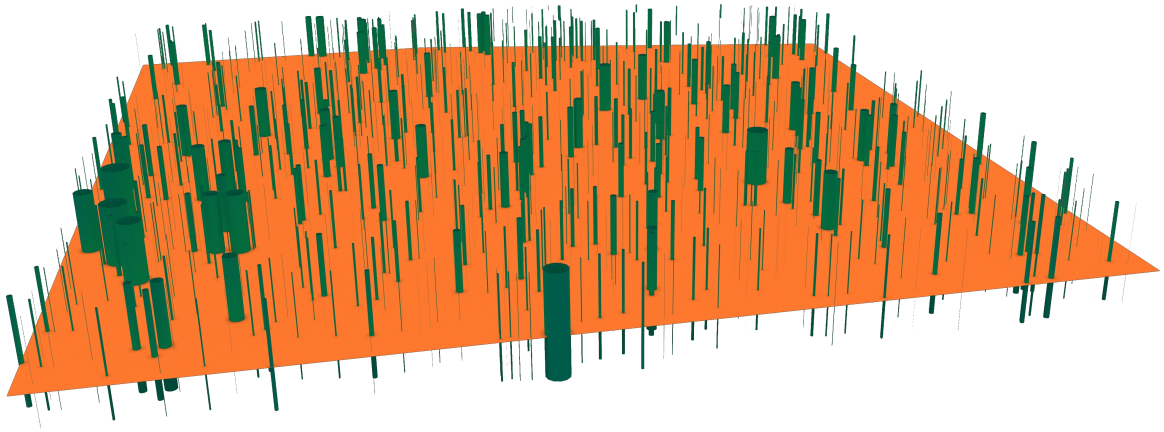

Figure 1. Rendering of the cylinder placement of one sample plot in Blender. The 50 × 50 m sample plot is orange and the cylinders following the Weibull distribution of tree diameters are green.

2.1.4. Simulated Laser Scanning

BlenSor is an add-on for Blender which allows the user to simulate various types of range scanners and other optical instruments [22]. It enables an efficient intersection of mathematical vectors (rays) with 3D objects defined in Blender and returns the range and the incidence angle. This information allows the user to calculate the number of rays possibly hitting an object at any distance from the origin of the ray (scanner location), or it can be used as a sampling procedure for visibility assessments of the sample plots.

2.1.5. Voxel Traversal Algorithm

We used a voxel traversal algorithm implemented by [23] based on the approach described by [24]. By knowing the starting point (scanner location) and the point where the laser beam (mathematical vector) hits an object, this algorithm can calculate, for every voxel in a predefined voxel grid, whether the vector entered a voxel or was stopped before entering the voxel. In this way, the algorithm returns, for a given set of rays, the number of rays entering each voxel and those intercepted (occluded) before reaching that particular voxel.

2.1.6. Visibility Assessment

Visibility assessment has a long tradition in GIS sciences for the evaluation of digital elevation models (e.g., [25,26]). Our approach is to use TLS simulations to assess the 2-dimensional visibility of forest stands. We use BlenSor to send out horizontal vectors from a virtual scanner position, following specific angular steps (angular resolution). From a statistical point of view, we sample the visibility of a given space (e.g., the sample plot) with the vectors and assess the visibility along each of the vectors by intersecting them with the objects (cylinders) within that space (see Figure 2). BlenSor returns the coordinates of the intersections within the sample plot or, in cases where there is no intersection, a coordinate of the vector outside the sample plot (red dots in Figure 2). The obtained dataset is

a 2D point cloud (or 3D point cloud with all the points in one plane). The voxel traversal algorithm described above evaluates for each voxel of a predefined voxel grid, the number of vectors entering and the number of vectors that could theoretically enter the voxel without occlusion. The visibility experiments, as described below, are conducted with vectors in a plane and the voxel space height is only one voxel, so one could also speak of "pixels" instead of "voxels". For the visibility assessment in this publication, we calculated, for each voxel, the ratio of rays entering the voxel to all the rays that theoretically could have entered the voxel. This is a measure of the visibility of a given voxel. We defined the mean of all these ratios within a plot as the mean relative visibility (V_m). We chose V_m as a measure of visibility because it takes every voxel into account, irrespective of the distance from the scanner.

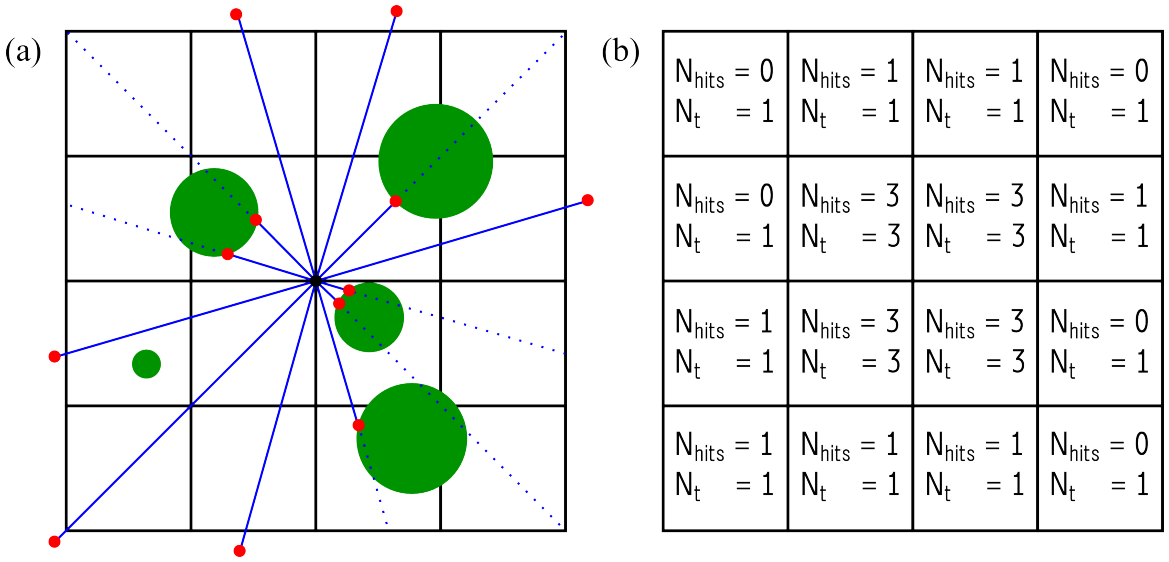

Figure 2. Illustration of visibility assessment. (**a**) Sample plot divided into a voxel (pixel) grid with scanner position in the centre. The cylinders are displayed as green circles, the unoccluded vectors as blue lines, the vectors occluded by the trees as dotted blue lines and the points of the point cloud as red dots; (**b**) The same sample plot showing, for each voxel (pixel), the number of vectors entering the voxel cell (N_{hits}) and the number of vectors that could enter the voxel cell without occlusion (N_t).

2.2. Theoretical Coverage of a Laser Scanning System in a 3D Space

The goal of this experiment was to determine the theoretical minimal coverage of a laser scanning system in a cubic space. The vertical extent of the sample plot was set to 50 m because that is the height of the tallest measured trees in the Swiss NFI.

We assumed the laser beam to be infinitesimally small in diameter. To define the direction in which these rays start, we assumed a scanning system with a rotating mirror on a horizontal axis. This mirror rotates again around a vertical axis, as applied in many commercial scanning systems, such as Faro Focus 3D and Leica BLK360, and in experimental systems such as SALCA [27]. In such a scanning system, the angular resolution refers to the angular steps in longitudinal and latitudinal directions. It leads to an increasing point density from the horizontal plane towards the zenith and the nadir. We tested angular scanning resolutions ranging from 0.01° to 1.00° (i.e., the angular resolutions in [°] of 0.01, 0.02, 0.04, 0.06, 0.1, 0.2, 0.5, 1). The location for the scanning system we chose to be the centre of the sample plot, at 1.3 m height above ground, corresponding to the height of the DBH measurement. To mimic variations in the object size, we varied the voxel size from 1 mm up to 1 m (i.e., the sizes in [m] of 0.001, 0.005, 0.01, 0.05, 0.06, 0.07, 0.1, 0.5, 1). To reduce the calculation time, we did not evaluate all the voxels in the voxel space but instead a maximum of 5000 randomly selected voxels for each scanner configuration.

As a measure of the coverage, we used the voxel traversal algorithm described in Section 2.1.5 to count the number of rays entering the sampled voxels (N_{hits}). As explanatory variables, we calculated, for each voxel, the Euclidean distance (D_e) from the voxel centre to the scanner location. To account for the effect of a higher point density towards the zenith and the nadir of the scanner, we derived the horizontal distance (D_h) to the scanner location. D_h is the distance, projected on the X–Y-plane, from the voxel centre to the scanner location. Additionally, we calculated the ratio of voxel size to scanner resolution ($R_{vs/sr}$). To test for the influence of D_e, D_h and $R_{vs/sr}$ on N_{hits}, we applied a linear regression using the software R [28]. Since all the variables are positive numbers, we log-transformed them following the recommendations of [29]. As some configurations with $R_{vs/sr}$ exhibited many voxels with N_{hits} of 0, we applied the regression on configurations starting at an $R_{vs/sr}$ of 1. At that point, every voxel in the 50 m cubic space obtains at least one hit, which allows the regression to be fitted in a meaningful way.

2.3. Influence of Stand Parameters on Visibility in a 2D Space

We used Blender to set up 2740 sample plots based on five annual NFI grids. For sampling visibility, we chose an angular resolution of 0.001°, which manifests a high sampling frequency. The voxel size was chosen considering two effects: if the voxel size is too small, the demand in computing power increases. However, large voxels overestimate the actual visibility. For the following experiments, we chose a voxel size of 0.1 m.

We calculated additional NFI-related stand parameters based on the generated diameter distribution files, to be used in the evaluation of the results. One parameter is the mean diameter of the 100 largest trees per hectare (D_{dom}). The other parameter is the stem number of the trees with a minimal diameter at breast height of 12 cm ($N_{tree \geq 12cm}$). To test the influence of the stand parameters, we transformed the dependent and independent variables, following the recommendations of [29]. Since the range of V_m is from 0 to 1, we applied an arc-sin-square-root transformation. The other variables were log-transformed. The software R [28] was used for the analysis.

2.4. Influence of the Scanning Location within Sample Plots on Visibility in a 2D Space

In this experiment, we investigated the influence of the scanning location within the sample plot on the visibility. We tested 25 evenly distributed scanning positions along the positive x-axis (T_h) of the local coordinate system. Another 25 scanner positions were tested following the diagonal (T_d) from the centre to the corner with coordinates (25, 25). Combined with the central scan, 51 scanner positions were tested in total (see Figure 3). In contrast to the other experiments where cylinders were set up with Blender, cylinders overlapping the scanner position were not relocated in this experiment. The affected sample plots were dropped from the sample to avoid alleys of visibility which would be generated on transects if the other approach was chosen. Due to computational constraints, we used the 537 stand samples from the last reporting period (2013) and not the full data set. Other than that, this experiment was set up identically to the former, using the same software tools. To test the influence of the scanner position, two additional independent variables were appended to the model described in the former experiment (see Equation (3)). We wanted to test the supplementary influence of the distance to the centre (D_c) and the transect (F_t) the scanner location belongs to. Both variables were added to the model, and D_c was log-transformed and squared. To visualize the influence of only these two variables, we removed the predicted values of the model using only the stand parameters from the actual V_m. The difference in V_m between the two transects we calculated as follows: first, we retransformed the residuals of the model with the stand parameters and D_c; second, we calculated the mean of these residuals for each transect. The difference of these means of residuals represents the mean difference in V_m without the influence of the stand parameters and D_c.

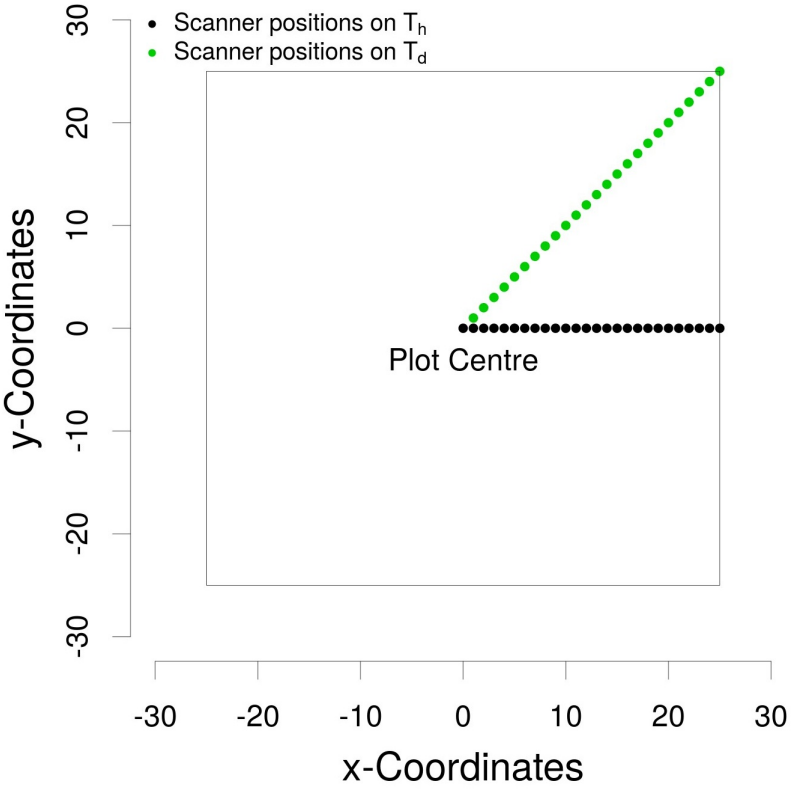

Figure 3. Locations of the tested scanner positions within the sample plot. T_h is the transect following the x-axis, T_d is the transect directed at a corner of the sample plot.

2.5. Influence of Scanner Location Patterns on Visibility in a 2D Space

The goal of this experiment was to show the influence of scanner location patterns (P_{sl}) on the visibility. A scanner location pattern is the combination of several scanning locations, as used for multiple terrestrial laser scanning acquisition. As in Section 2.4, we used the stand parameters of one annual NFI sampling grid. Various (P_{sl}) are described in the literature. Some authors [11,14,30–32] describe multiple scanning patterns, where most of the scanner locations are on the edge of the sample plot. Others [33–36] placed the scanner at multiple locations outside of the sample plot, either to scan isolated stands or to scan within a larger stand. On the other hand, a third group of authors [9,37–41] applied various scanner location patterns, such as one scan in the centre and four to six around it, or distributed the scanner locations evenly. Based on these scanner location patterns, we defined 25 scanning locations that could be combined to form various scanner location patterns (see Figure 4). We also added very close scanning locations to test the effect of very dense scanner patterns (e.g., a brute force approach). Due to computational constraints, we restricted testing of the patterns we found in the literature and only added specific scanner location patterns to learn about the effect of shifting one scanning location. The complete set of tested scanner location patterns is shown in the Appendix A in Figures A2 and A3. Due to the combination of multiple scanner locations with their associated 2D point clouds, we calculated the visibility (V_m) in the following way: For each scanning location to be used in a pattern, we calculated the invisible fraction of each voxel (F_i). F_i is one minus the ratio of rays entering the voxel to the number of rays that could have entered the voxel in case of no occlusion. To combine the visibility of the various scanner locations, we assumed that every additional scan reduces the initial F_i in (actuarial) expectation in the ratio of F_i of the newly added scan. So the V_m of n combined scans is calculated as showed in Equation (1).

$$V_m = 1 - (F_{i(1)} * F_{i(2)} * ... * F_{i(n)}) \quad (1)$$

To check for the influence of the number of positions (N_s) used for a scanning pattern and the scanner location pattern (P_{sl}), we added these variables to the basic equation with the stand parameters (see Equation (3)). We log-transformed N_s following the recommendations of [29]. We compared the efficiency of the various P_{sl} without the influence of the stand parameters and N_s (see Figure 5). To do so, we fitted the basic model (Equation (3)) including N_s using the software R [28]. With this model, we predicted V_m for all the sample plots. We subtracted this value from the "measured" V_m and normalised these values by subtracting the mean V_m of the single scanner locations in the centre of the sample plot. We call this value "scan location pattern efficiency" (P_{sl}-efficiency).

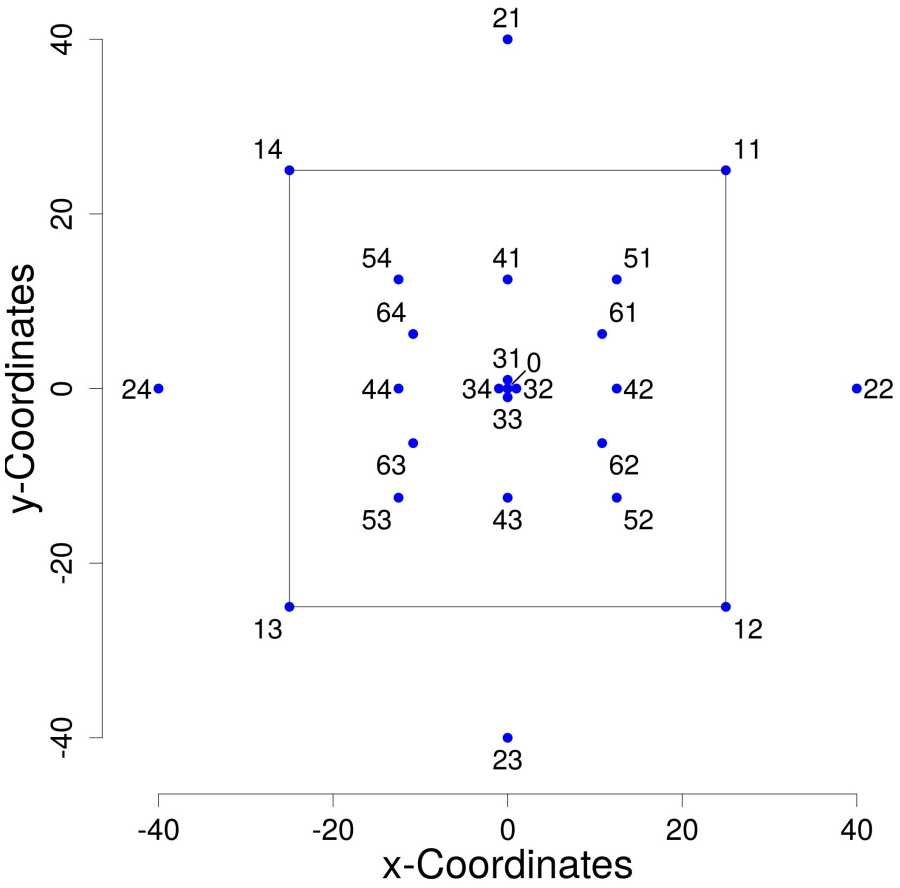

Figure 4. The scanning locations tested in each sample plot of 50 × 50 m. The displayed scanning locations, with their identification number, can be combined to form scanning location patterns for the search for efficient patterns, which are each evaluated for occlusion and coverage (visibility).

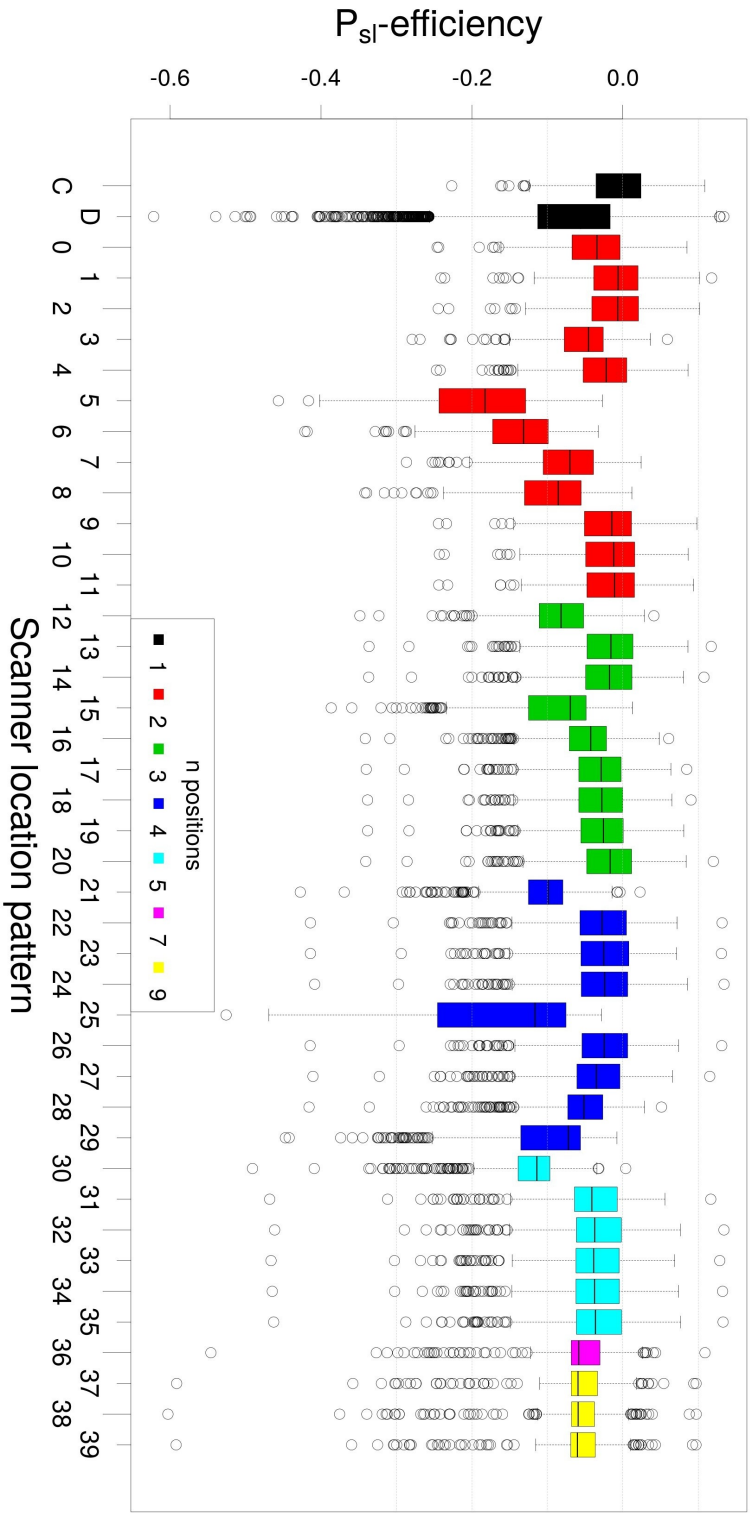

Figure 5. Efficiency of the scanner location patterns (P_{sl}-efficiency). P_{sl}-efficiencies are the residuals of the V_m model explained by the stand parameters and the number of combined scanner locations, normalised to the mean V_m of single scans in the centre of the sample plots. The figure shows the change in efficiency compared with that of the central scan (C) when different scanner location patterns are applied. The scanner location pattern "C" is the single central scan and "D" is the mean of all the other tested single scan positions that were used for the patterns.

3. Results

3.1. Theoretical Coverage of a Laser Scanning System in a 3D Space

To investigate the theoretical coverage of a TLS system in a cubic space with an edge length of 50 m, we simulated laser range measurements with geometric vectors as a proxy for TLS laser pulses. As a proxy for object size, we used the size of voxels in the given 3D space. The number of laser beams (vectors) entering each voxel N_{hits} served as a measure of coverage, i.e., detection quality of the laser scanner. With a sufficient resolution, any size of object could theoretically be resolved throughout the scene, i.e., at any distance to the scanner, given, that the laser beam has no extent (footprint). Besides the Euclidean distance D_e and the horizontal distance D_h from the voxel centre to the scanner location, we used the ratio of voxel size to scanner resolution ($R_{vs/sr}$) as an independent variable to explain N_{hits}. For a proper applicability of a linear regression, we only used settings where every voxel in the cubic space of 50 m has at least one vector passing it. Figure 6 shows that, in the given experimental setting, this point is reached when $R_{vs/sr}$ is equal to 1.

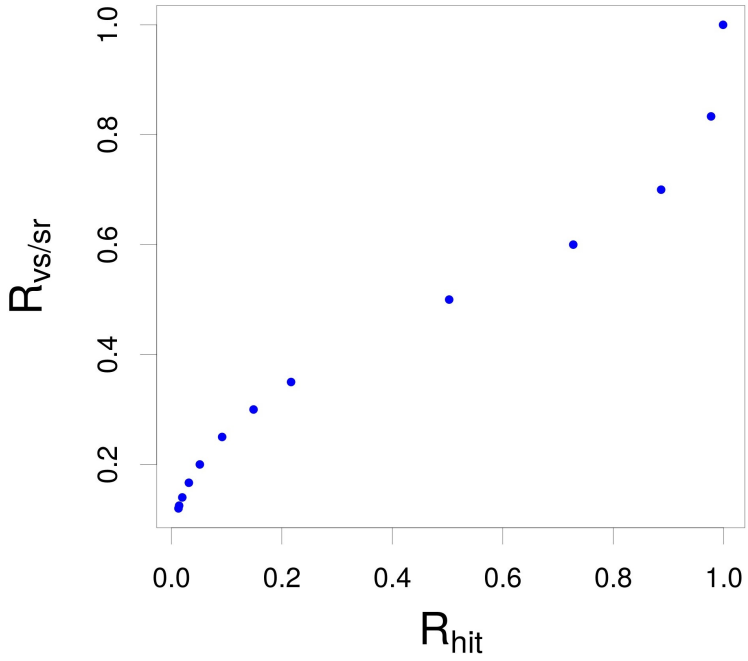

Figure 6. The relationship between the ratio of voxel size to scanner resolution [m/°] ($R_{vs/sr}$) and the ratio of the number of voxels hit by at least one ray to all the voxels in the cubic space with edge size of 50 m (R_{hit}).

The regression was conducted using the following formula:

$$log(N_{hits}) = log(D_h) + log(D_e) + log(R_{vs/sr}) \quad (2)$$

The regression showed a very good performance, with all variables highly significant and an adjusted R^2 of 0.99. Table 1 displays the coefficients of the independent variables and their respective p values.

In Table A1 in the Appendix A, the mean number of hits per voxel in the various ratio classes and the (Euclidean) distance to the scanner are shown.

Table 1. Model coefficients and standardised model coefficients based on scaled variables to make their effect sizes comparable.

Variable	Model Coefficient	Standardised Model Coefficient	*p* Value
Intercept	8.38	0	<0.0001
log (D_h)	−0.9	−0.22	<0.0001
log (D_e)	−1.09	−0.18	<0.0001
log ($R_{vs/sr}$)	2.03	0.92	<0.0001

3.2. Influence of Stand Parameters on Visibility in a 2D Space

The hypothesis was that the structure of a stand, represented by a Weibull distribution, stem number and dominant diameter (D_{dom}), would have an influence on the visibility within the stand. D_{dom} is the mean diameter of the 100 largest trees per hectare. To test this hypothesis, we randomly placed cylinders following Weibull distributions derived from 2740 sample plots of the Swiss NFI from the year 2009 to 2013. The number of placed cylinders ranges from 30 to 19,620 (see Figure 7). The scale parameter of the Weibull distribution ranges from 0.002 to 65.8 and the shape parameter ranges from 0.2 to 9.8. To analyse the visibility, the mean relative visibility of voxels (V_m) in each 50×50 m plot was calculated. The relative visibility of a voxel is the ratio between the vectors emitted from the virtual scanner location (that either passed the voxel or hit an object within that voxel) and the theoretical number of vectors that could pass the voxel in a space without occluding objects. To account for the occurring range in the variables, they were transformed following the recommendations of [29].

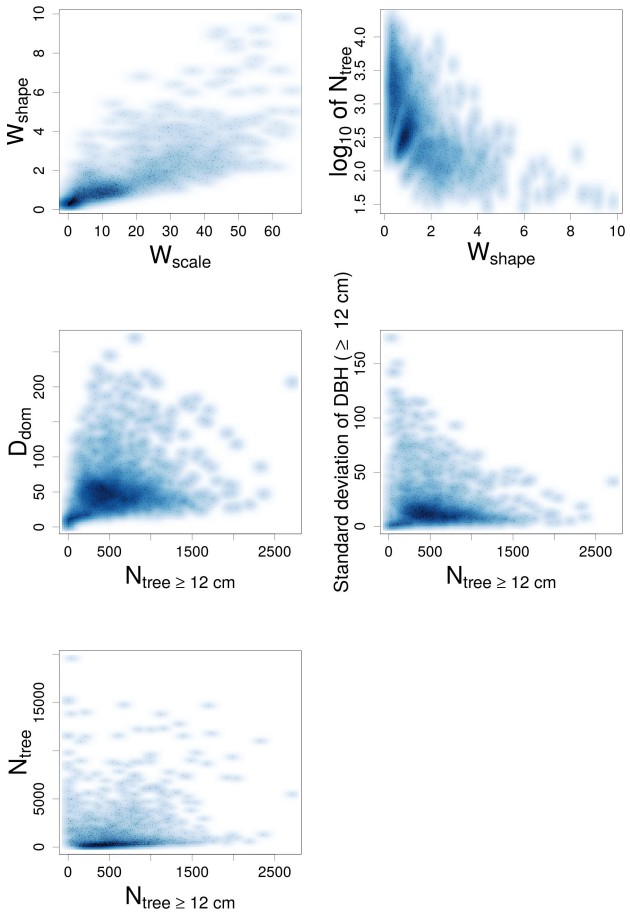

Figure 7. Derived stand parameters from National Forest Inventories (NFI) data and their relationship to each other.

The regression was conducted using the following formula:

$$\arcsin(\sqrt{V_m}) = log(N_{tree}) + log(W_{shape}) + log(W_{scale}) + log(D_{dom}) + log(N_{tree \geq 12cm}) \quad (3)$$

All the independent variables except the Weibull scale parameter (W_{scale}) are highly significant, with an adjusted R^2 of 0.96. The refitted model without W_{scale} led to the coefficients shown in Table 2. In Figure A1 in the Appendix A, the distribution of V_m for different D_{dom} and N_{tree} classes is shown.

Table 2. Model coefficients and standardised model coefficients based on scaled variables to make their effect size comparable.

Variable	Model Coefficient	Standardised Model Coefficient	*p* Value
Intercept	2.726	0	<0.0001
$log(N_{tree})$	−0.249	−1.211	<0.0001
$log(W_{shape})$	−0.124	−0.384	<0.0001
$log(D_{dom})$	−0.116	−0.271	<0.0001
$log(N_{tree \geq 12cm})$	0.008	0.06	<0.0001

3.3. Influence of the Scanning Location within Sample Plots on Visibility in a 2D Space

To test the influence of the scanner position within the sample plot, we tested 51 scanner positions (see Figure 3). To confine computational cost, we reduced the dataset by using only the NFI plots surveyed in 2013, ending up with 537 different stand parameters. The regression of this reduced dataset leads to the same R^2 and to very similar coefficients and significance values (compare Table 2 earlier in the text with Table A2 in the Appendix A). To test the influence of the scanner position within the sample plot, we added the distance to the plot centre (D_c) and a factor F_t which describes the kind of transect (horizontal or diagonal) the tested scanner position is situated on. The applied model is as follows:

$$\arcsin(\sqrt{V_m}) = log(N_{tree}) + log(W_{shape}) + log(D_{dom}) + log(N_{tree \geq 12cm}) + log(D_c) + log(D_c)^2 + F_t \quad (4)$$

All the added independent variables were significant, and the whole model showed an R^2 of 0.94. When reducing V_m by the influence of the stand parameters and the distance to the centre, the transect following the x-axis had on average, a V_m of 0.013 greater than that of the diagonal transect. Figure 8 shows the reduction in V_m caused by the distance to the centre.

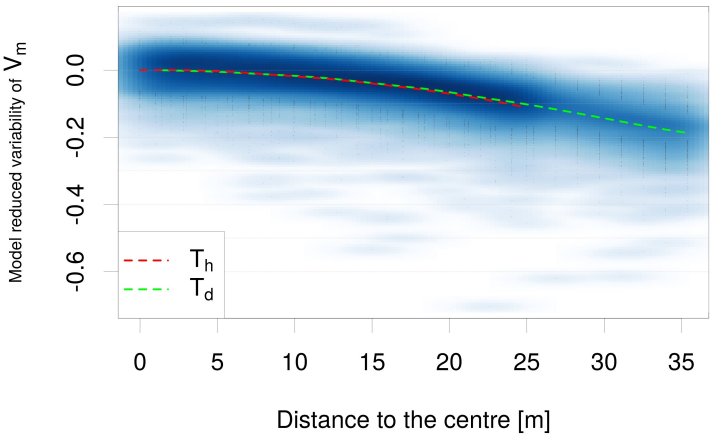

Figure 8. Reduction in visibility within the sample plot due to increased distance of the scanner location from the plot centre. V_m is reduced by the influence of the stand parameters and normalised to the mean V_m of the scans in the plot centre. T_h is the transect following the x-axis, T_d is the transect directing to a corner of the sample plot.

3.4. Influence of Scanner Location Pattern on Visibility in a 2D Space

The combination of multiple scanner positions reduces the occlusion in a stand substantially [17,34,42,43]. Based on scanner location patterns found in the literature, we simulated 25 single scanning positions on each sample plot (n = 536) (see Figure 4) and combined them to form a total of 40 scanning location patterns (see Figures A2 and A3 in the Appendix A).

Figure 9 shows the differences in the mean visibility V_m caused by varying the number of scanner positions. As one would expect, increasing the number of scans (N_s) has a positive influence on the quality of the point cloud by covering more of the sampled area. Our evaluations showed that the number of positions has a strong and significant influence on the mean visibility of the stand. We added the number of scanning locations (N_s) to the basic model (Equation (3)). The model produced an R^2 of 0.92. If we conduct the same procedure with the scanner location patterns (P_{sl}), the corresponding tested model has an R^2 of 0.94. Table 3 displays the mean visibility for each P_{sl}. Since P_{sl} includes N_s implicitly, these two R^2 figures imply that the kind of pattern chosen has an influence on the visibility within the stand as well. Figure 5 shows the change in visibility of the tested P_{sl} compared to a single scan in the centre of the sample plot. In the Appendix A we show, for each of the most efficient P_{sl}, the histrogram of visibility by classes of D_{dom} and N_{tree} (Figures A4–A9) . Following the findings given above, V_m becomes higher as more scans are combined and as N_{tree} becomes lower. Stem number class 3 (501 to 1000 trees per hectare) and 4 (more than 1000 trees per hectare) seem to be especially sensitive to the scanning regime.

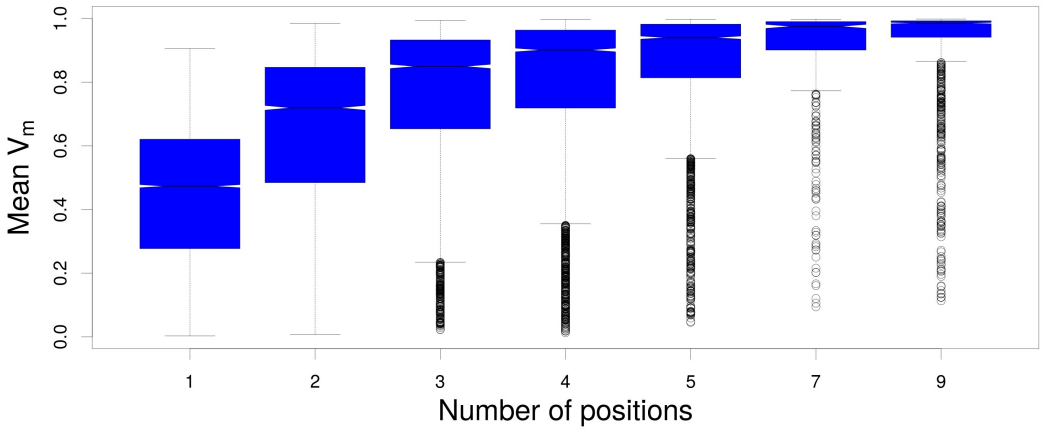

Figure 9. Influence of the number of combined scanning locations (N_s) on the mean visibility (V_m) within the plot.

Table 3. Changes in the mean visibility (V_m) influenced by scanner location pattern.

Scanner Location Pattern	Combined Locations	Mean V_m	Standard Deviation of V_m
0	32, 34	0.67	0.23
1	63, 61	0.69	0.24
2	42, 44	0.69	0.24
3	22, 24	0.65	0.25
4	51, 53	0.68	0.24
5	11, 13	0.52	0.26
6	11, 51	0.57	0.24
7	11, 0	0.63	0.25
8	11, 53	0.61	0.25
9	42, 32	0.68	0.24
10	42, 0	0.69	0.24
11	42, 34	0.69	0.24
12	0, 34, 32	0.72	0.22

Table 3. *Cont.*

Scanner Location Pattern	Combined Locations	Mean V_m	Standard Deviation of V_m
13	0, 61, 63	0.78	0.23
14	0, 51, 53	0.78	0.23
15	0, 11, 13	0.71	0.26
16	53, 43, 52	0.75	0.23
17	53, 33, 52	0.77	0.23
18	53, 0, 52	0.77	0.23
19	53, 31, 52	0.77	0.23
20	53, 41, 52	0.78	0.23
21	31, 32, 33, 34	0.76	0.21
22	61, 62, 63, 64	0.84	0.21
23	41, 42, 43, 44	0.84	0.21
24	51, 52, 53, 54	0.84	0.21
25	11, 12, 13, 14	0.71	0.28
26	51, 62, 53, 64	0.84	0.21
27	51, 61, 53, 63	0.83	0.22
28	33, 43, 52, 62	0.81	0.22
29	11, 12, 13, 0	0.76	0.26
30	0, 31, 32, 33, 34	0.78	0.21
31	0, 41, 42, 43, 44	0.86	0.2
32	0, 51, 52, 53, 54	0.87	0.19
33	62, 51, 52, 53, 54	0.87	0.2
34	42, 51, 52, 53, 54	0.87	0.2
35	32, 51, 52, 53, 54	0.87	0.19
36	0, 41, 61, 62, 43, 63, 64	0.9	0.17
37	53, 43, 52, 44, 0, 42, 54, 41, 51	0.92	0.15
38	53, 43, 52, 44, 0, 42, 54, 41, 11	0.92	0.16
39	53, 43, 52, 44, 0, 42, 54, 41, 61	0.92	0.15

4. Discussion

4.1. Theoretical Coverage of a Laser Scanning System in a 3D Space

The first goal of this study was to test the link between scanner resolution and a minimum object size that could theoretically be detected without accounting for occlusion, given the assumption of an infinitesimally small laser beam. We provided a model which includes the independent variables "distance to the scanner" (D_e), "horizontal distance to the scanner" (D_h) and "ratio of object size to scanner resolution" ($R_{vs/sr}$), which enables calculation of the number of possible rays passing through a voxel with very high precision (R^2 of 0.99). The last bit of unexplained variation in the model possibly comes from the fact that the cross section of the voxel from the direction of the assumed scanner position varies, depending on the direction from which a voxel is scanned. Starting at ($R_{vs/sr}$) > 1, every object of the respective size obtains at least one hit by a laser ray in a 50 m cube. Below that value, the ratio between the number of voxels with at least one hit by a laser and the total number of voxels decreases in a close-to-linear s-shaped connection to $R_{vs/sr}$ (see Figure 6). As mentioned above, this experiment respects neither the influence of a laser beam divergence nor any effect of occlusion by other objects in the same scene. Nevertheless, a laser beam with an increasing diameter when crossing the forest scene can hit multiple objects at the same time, leading to various effects in respect to the obtained point clouds. Depending on the technology used, this can deliver point clouds with worse quality concerning the distance to the object or, in the better case, can deliver multiple returns from one single laser pulse. However, this experiment can support decisions for a field campaign concerning the size of the object of interest and the corresponding minimal scanner resolution. Findings from this experiment allow users to calculate in advance the maximum possible number of laser beams hitting an object of a specific size in any direction and distance to the scanner. This is especially important for measurements of tree parts which scanners cannot be placed close to, e.g., branches higher up in

the canopy. For these objects, only multiple TLS measurements can improve the coverage, albeit in a linear fashion. Newnham et al. [42] identify two different categories of data retrieval approaches from TLS generated point clouds: gap probability and geometrical modelling. While the former approach samples the forest scene to provide a complement of all vegetation components, the latter uses the discrete point clouds to derive geometrical properties of the scanned object, e.g., by quantitative structure modelling (QSM) [44,45]. The suitability of geometrical modelling depends on a sufficient point based representation of an object in order to infer the geometric properties. Our results suggest that geometric modelling is more suitable for the lower forest layer(s), while in the top layers the point density might be too low simply because of the (vertical) distance to the scanner, not even considering occlusion.

4.2. Influence of Stand Parameters on Visibility in a 2D Space

The experiment to explore the influence of stand parameters on visibility showed that the Weibull parameter "shape" (W_{shape}) has a significant influence on V_m of a stand. The number of trees (N_{tree}), the mean diameter of the 100 largest trees per hectare (D_{dom}) and the number of trees with a DBH of $\geq$12 cm ($N_{tree \geq 12cm}$) show a highly significant influence as well. On the other hand, the Weibull "scale" parameter (W_{scale}) in combination with the above-mentioned stand parameters has no influence. The standardised model coefficients, shown in Table 2, reveal the magnitude and the direction of the influence. The number of trees clearly has the strongest (negative) influence, followed by the W_{shape} parameter and D_{dom}. Surprisingly, $N_{tree \geq 12cm}$ has a positive relationship with V_m. A reason for this finding could be that there is some interaction with the other variables that alleviates their influence slightly. However, the standardised model coefficient shows that this influence is very small and not relevant. The independent variables of the model based on NFI data have a very high variability, due to the fact that only a few trees of a stand are located within the NFI sample plot. Their occurrence is subject to a stochastic process. This means that the stand description derived from the NFI data is not the actual description of the stand, but an unbiased expectation over a large sample of plots. The possible variety of stands that could occur is covered, or even goes beyond realistic occurrences. In the experiments of this publication, other influences are not considered, such as uneven terrain, lying dead wood or foliage, twigs and branches. However, twigs and branches might have a similar influence on visibility as a high number of small (stem) cylinders.

The assessment of visibility in this experiment is based on range measurements of geometric vectors with an infinitesimally small diameter. Especially when small objects with unsuitable angular resolution are scanned, a fraction of these objects would theoretically be invisible for the laser scanner (Figure 6). As mentioned above, laser pulses of any TLS device have a starting diameter and a beam divergence. Due to this increasing diameter (footprint) of the laser beam, a single laser pulse can hit multiple objects at the same time. Therefore, small objects would often be hit by a laser beam with a footprint, which could lead to noise or additional information in the acquired point cloud depending on the LiDAR technology of the TLS device (phase shift or time of flight). Kükenbrink et al. [23] noticed an overestimation of occluded volume when laser scanning data were simulated using an infinitesimally small laser beam diameter.

The applied model (Equation (3)) shows a relatively high adjusted R^2 of 0.96. The unexplained variation might arise from the location of the scanner with respect to its neighbouring trees (cylinders) or might be due to the placement process of the cylinders. In this study, we chose a Poisson process to place them. Theoretically, it would be possible to apply so called "point processes", which are based on empirical data of tree distributions, to which the NFI data cannot contribute, due to the small sample plot size [46–48]. Even though the Weibull distribution is a common choice to describe diameter distributions of stands [20], it does not encompass distributions with more than one local maximum, as described in [12]. This experiment supports the assumption that, on the one hand, the number of objects and, on the other hand, the size of the objects, represented as D_{dom} and W_{shape}, influence visibility the most. With the derived formulas, we are now able to assess the extent of the influence

of these stand parameters in advance. The experiment was conducted in a 2D space. This is useful for any application that is applied in such a setting, for example certain methods of stem detection or DBH derivation, as described by [34,37,39,49,50]. However, most current methods of feature extraction are based on 3D point clouds, so it is questionable to what extent the findings of this 2D experiment can be transferred to a 3D space.

What kinds of stands are covered by the Weibull parameters used here? The Weibull distribution with a shape parameter (W_{shape}) of 1 describes an exponential distribution, whereas with W_{shape} 3.6 it follows a normal distribution. With a larger W_{shape}, the distribution becomes more negatively skewed. Figure 7 illustrates the combinations of W_{shape} with W_{scale} and N_{tree}. The plots show that the simulated stands include typical regeneration stands with a large number of trees (low W_{shape}, low W_{scale}), uneven-aged stands (W_{shape} around 3.6 and large W_{scale} around 50) to relatively even-aged mature stands (large W_{shape}, large W_{scale}). These Weibull parameters are based on the same data that were used to produce the online publication of the Swiss NFI results [51].

4.3. Influence of the Scanning Location within Sample Plots on Visibility in a 2D Space

By simulating different scanning locations, we showed the effect of the scanner placement within a sample plot on occlusion and coverage. We proved that the most efficient location to place a scanner in a single-scan setup is the centre of a sample plot, as one would intuitively assume. The mean visibility (V_m) within the plot decreases when the scanner is placed at an increasing distance from the plot centre. Whether the scanner is moved towards an edge or to a corner only makes a small difference. The reason for this effect is that the further away the scanner is from the plot centre, the longer the distance a laser beam has to travel to scan the opposite side of the sample plot and the more likely it is that the beam is intercepted by tree trunks. A limitation of this experiment was that no location outside of the plot was tested. In a continuous forest, the effect of increasing occlusion is very likely to continue with larger distances. If the stand is isolated in a non occlusive surrounding, the outside view may not lose visibility because no additional occluding objects will cross the view line of the scanner. Figure 8 shows the remaining unexplained variation of the mean visibility V_m. This could be either due to the random placement of the cylinders or due to the placement of the scanner relative to its nearest neighbouring cylinders, as mentioned above.

4.4. Influence of Scanner Location Pattern on Visibility in a 2D Space

With the fourth experiment, we tested the influence of multiple scanning locations on the visibility within sample plots. We evaluated 40 scanning location patterns and showed that, on average, every additional scan increased the visibility (see Figure 9). However, there is a saturation effect: for larger numbers of combined scans, the additional gain in V_m decreases. Nevertheless, the different patterns of scanner positions showed considerable differences in efficiency (see Figure 5). The least favourable pattern is scanning from the edge (as with P_{sl} 5 or 25, see Figures A2 and A3), which leads to a strong reduction in visibility. Similarly, very close P_{sl} (as in P_{sl} 0, 21 or 30) seem to deliver a low visibility compared to other patterns. Another loss of efficiency, though not to the same extent as those mentioned above, seems to occur with an uneven distribution of scanning locations over the sample plot (as in P_{sl} 6, 16 or 28). From P_{sl} 16 to 20, such an unevenness decreases continuously and efficiency increases. Minor shifts of a few metres (as in P_{sl} 18 to 19 or 9 to 10 to 11) do not worsen V_m notably. Even more severe shifts of the central position, as tested in P_{sl} from 32 to 35, do not show relevant changes in efficiency.

As an overall conclusion from the analysis of the scanner location patterns, the following rule of thumb could be inferred: an even distribution of scanner locations over the sample plot with even distances to the edge of the sample plot and to other scanner locations delivers the best visibility of the stand. Additionally, a local adjustment of the scanner location aimed at increasing the distance to the closest surrounding trees would not affect V_m; on the contrary, it would likely bring a gain in efficiency, as [14] stated.

5. Conclusions

In this study, we investigated the maximal possible coverage of a TLS device in a 50 m cubic voxel space. Additionally, using NFI Data and a 3D content creating suite, we analysed the influence of stand parameters, the scanning location within a sample plot and scanner location patterns on the visibility within a sample plot of 50×50 m.

We found a close relationship between the number of infinitesimally small laser beams hitting an object and the angular scanner resolution, the object size, and the distance to the scanner. These findings will help to exclude unrealistic expectations in TLS measurements. The number of trees clearly has the strongest influence on the visibility of a sample plot. Parameters with the second and third strongest influence on visibility are the shape of the Weibull distribution and the mean diameter at breast height of the 100 largest trees per hectare. These results suggest that, depending on the stand, different scanning settings might be necessary. The most efficient scanner location in terms of visibility is the centre of the sample plot. If multiple locations are used, our results show that an even distribution of the scanner locations over the sample plot, with even distances to the edge of the sample plot and to other scanner locations, delivers the best visibility for deriving properties of the stand. A local adjustment of the scanner location considering the surrounding trees could contribute to an even better visibility.

These findings will contribute to efficient TLS applications within forest inventories.

Acknowledgments: This study is fully financed by the Swiss National Forest Inventory.

Author Contributions: Meinrad Abegg designed the experiments, conducted the analysis and wrote the paper. Daniel Kükenbrink contributed the code for the voxel traversal. Jürgen Zell derived the Weibull parameters from the NFI data and assisted with the interpretation of the statistics. Michael Schaepman contributed to the design of the form and the content of the publication. Felix Morsdorf contributed ideas and reviewed the manuscript.

Conflicts of Interest: The authors declare no conflict of interest.

Abbreviations

The following abbreviations are used in this manuscript:

D_c	Horizontal distance to the centre of the sample plot
DBH	Diameter at breast height
D_{dom}	Diameter of the dominant (the largest) 100 trees per hectare
D_e	Euclidean distance from the voxel centre to the scanner location
D_h	Horizontal distance from the voxel centre to the scanner location
GIS	Geographical information system
LiDAR	Light detection and ranging
NFI	National Forest Inventory
N_{hits}	Number of rays (vectors) entering a voxel
N_s	Number of scanning locations combined to a scanner location pattern
N_t	Number of rays (vectors) that could enter a voxel without occlusion
N_{tree}	Number of trees per hectare with a minimal height of 1.3 m
$N_{tree \geq 12cm}$	Number of trees per hectare with a minimal DBH of 12 cm
P_{sl}	Scanner location pattern: The pattern multiple scanning locations are combined to scan a sample plot
$R_{vs/sr}$	Ratio of voxel size [m] to scanner resolution [°]
TLS	Terrestrial Laser Scanning
T_h	Horizontal transect within the sample plot. The transect following the positive x axis of the local coordinate system
T_d	Diagonal transect within the sample plot, ranging from the plot centre to the corner of the sample plot with coordinates (25,25)
V_m	Mean visibility of the sample plot
W_{scale}	Weibull scale parameter
W_{shape}	Weibull shape parameter

Appendix A

Table A1. Mean hits by (Euclidean) distance class and ratio voxel size to scanner resolution ($R_{vs/sr}$) class.

	$R_{vs/sr}$-Class					
	0–0.49	**0.5–0.9**	**1–4.9**	**5–9.9**	**10–49.9**	**>50**
Distance Class						
0–4.9	14.9	295	3203	30,744	279,571	4,653,479
5–9.9	1.8	41	457	4453	38,371	610,737
10–14.9	0.5	15	174	1695	14,538	230,408
15–19.9	0.2	8	93	909	7770	123,584
20–24.9	0.1	4	58	575	4945	78,485
25–29.9	0	3	40	400	3451	54,917
30–49.9	0	1	22	221	1913	30,431
>50	0	0	8	89	779	12,420

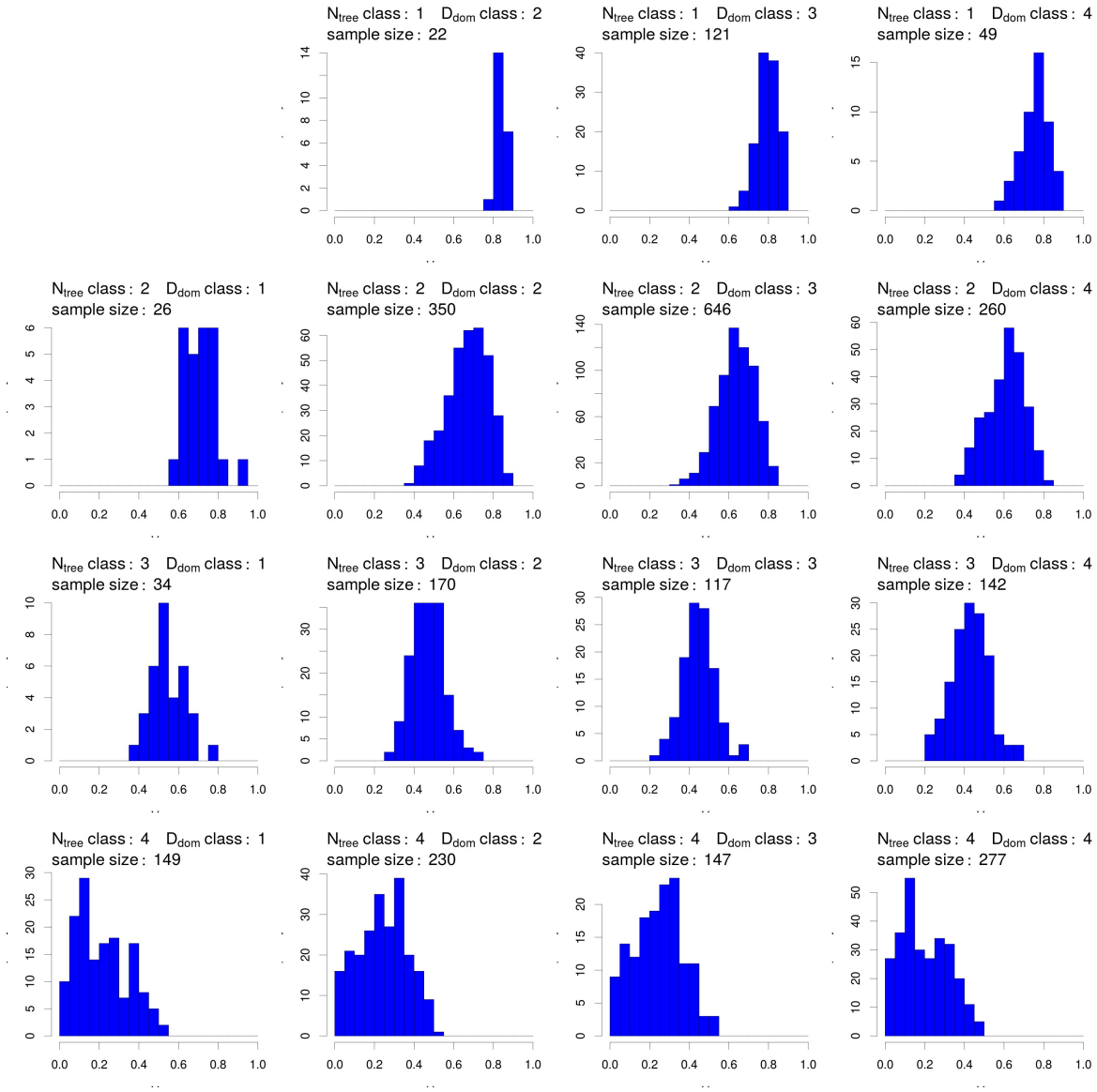

Figure A1. Visibility (V_m) by stand types. D_{dom} class 1 ($D_{dom} \leq 20$), D_{dom} class 2 ($D_{dom} > 20$ and ≤ 40), D_{dom} class 3 ($D_{dom} > 40$ and ≤ 60), D_{dom} class 4 ($D_{dom} > 60$), N_{tree} class 1 ($N_{tree} \leq 100$), N_{tree} class 2 ($N_{tree} > 100$ and ≤ 500), N_{tree} class 3 ($N_{tree} > 500$ and ≤ 1000), N_{tree} class 4 ($N_{tree} > 1000$).

Table A2. Model coefficients explaining V_m on a single annual NFI grid. R^2 = 0.96.

Variable	Model Coefficient	Standardised Model Coefficient	*p* Value
Intercept	2.781	0	<0.0001
$log(N_{tree})$	−0.251	−1.23	<0.0001
$log(W_{shape})$	−0.13	−0.408	<0.0001
$log(D_{dom})$	−0.123	−0.285	<0.0001
$log(N_{tree \geq 12cm})$	0.006	0.047	<0.0001

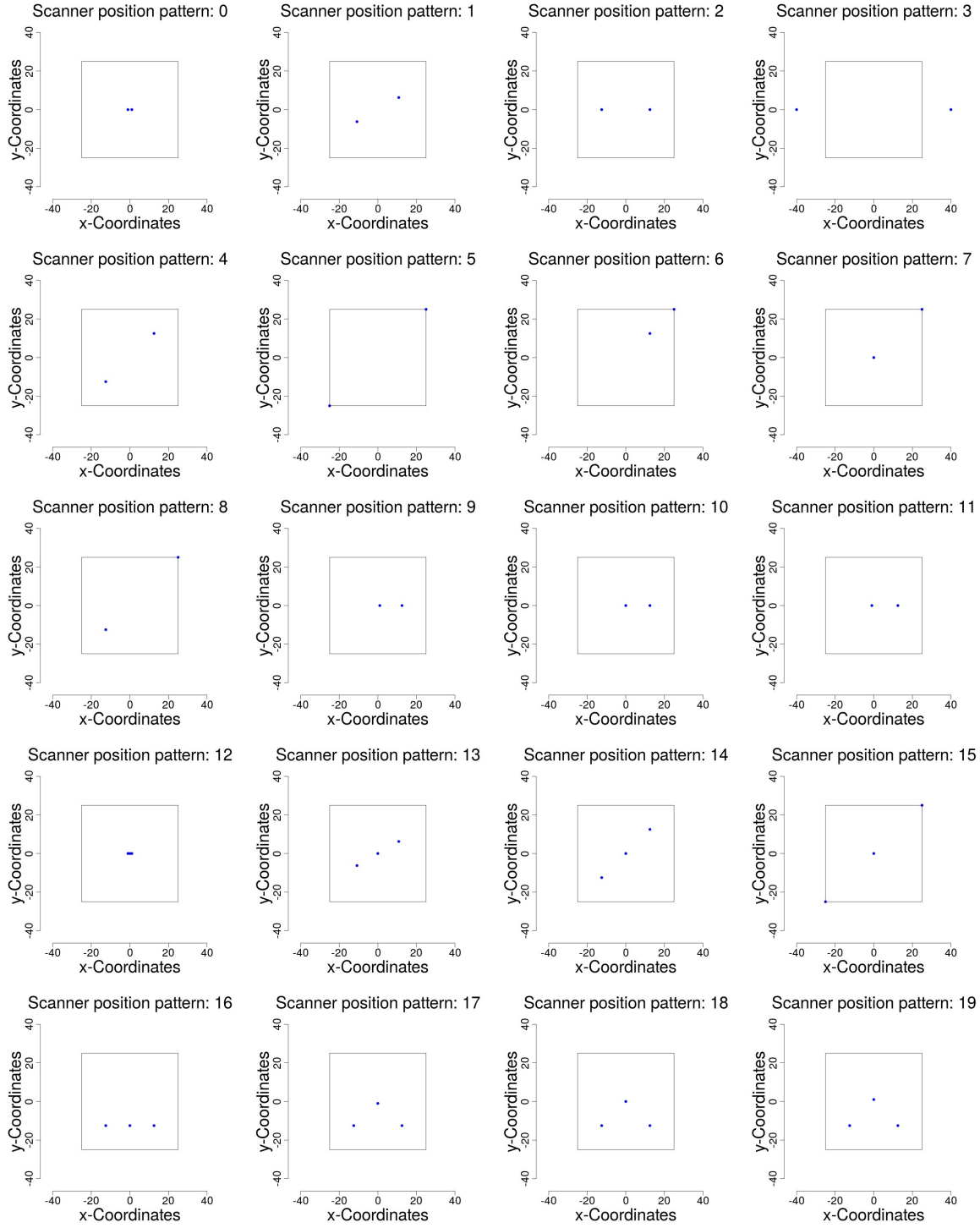

Figure A2. Tested scanner location patterns 0 to 19.

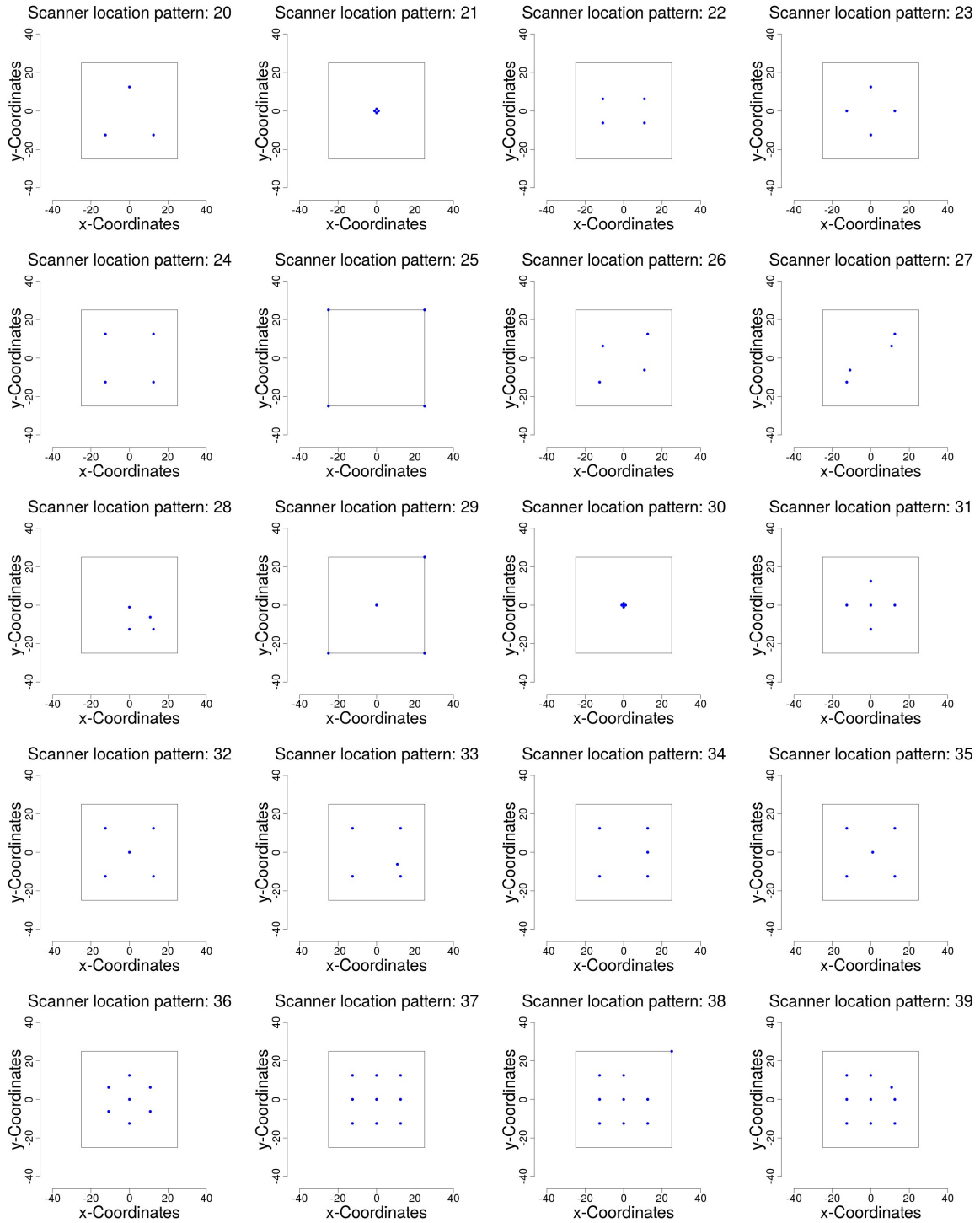

Figure A3. Tested scanner location patterns 20 to 39.

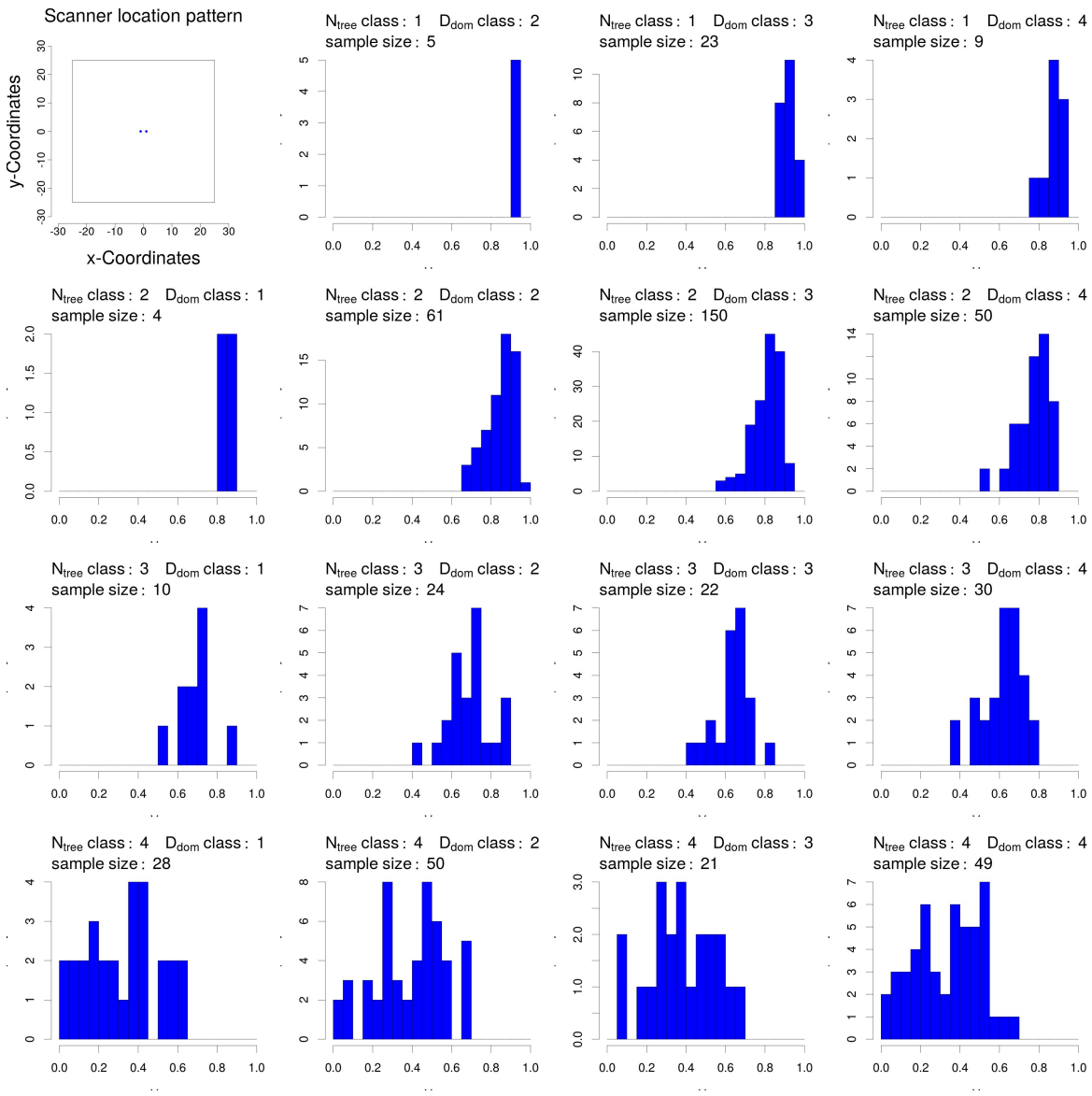

Figure A4. Visibility (V_m) of scanner location pattern 0 in dependence of D_{dom} class and stem number class. D_{dom} class 1 ($D_{dom} \leq 20$), D_{dom} class 2 ($D_{dom} > 20$ and ≤ 40), D_{dom} class 3 ($D_{dom} > 40$ and ≤ 60), D_{dom} class 4 ($D_{dom} > 60$), N_{tree} class 1 ($N_{tree} \leq 100$), N_{tree} class 2 ($N_{tree} > 100$ and ≤ 500), N_{tree} class 3 ($N_{tree} > 500$ and ≤ 1000), N_{tree} class 4 ($N_{tree} > 1000$).

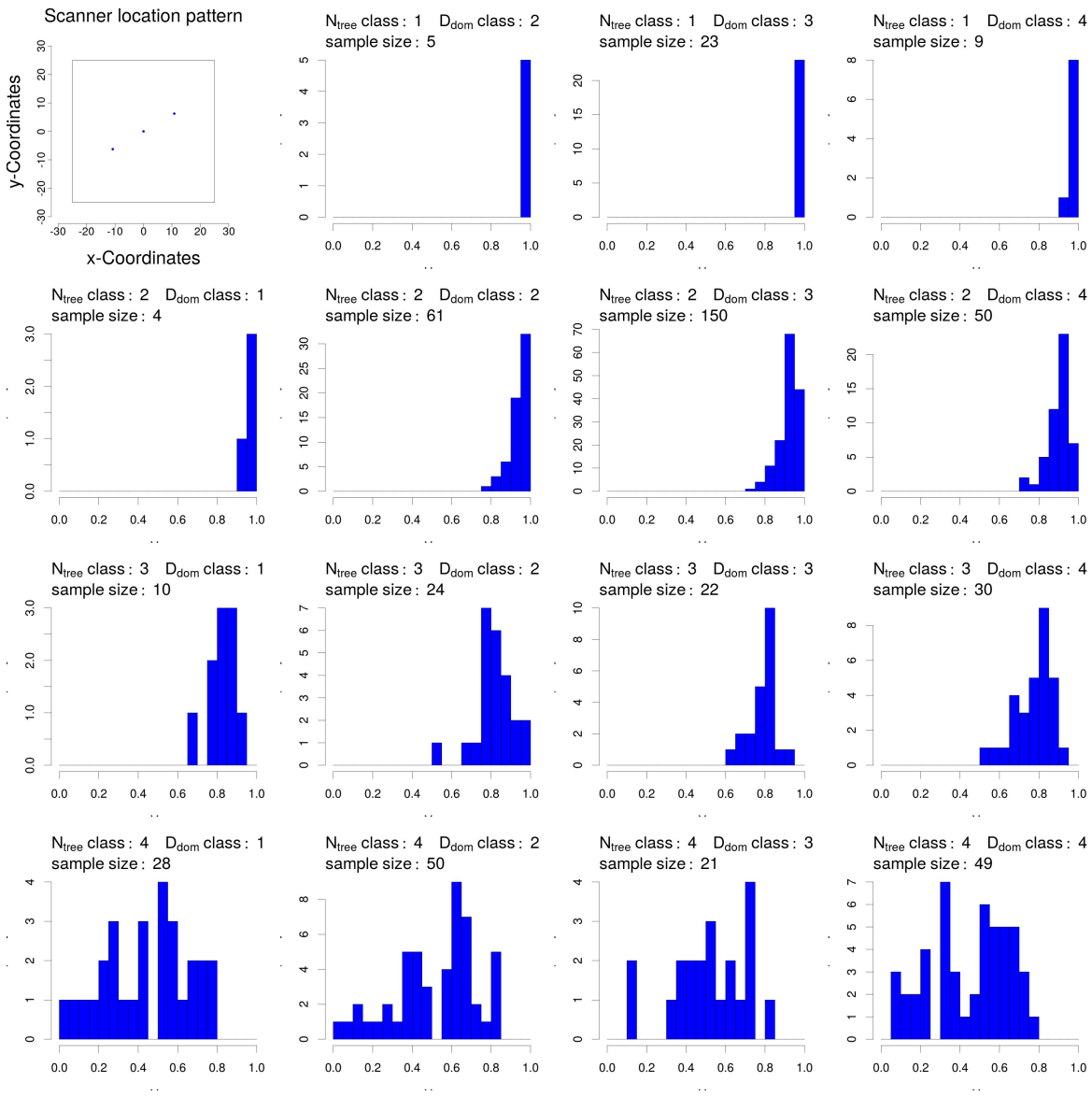

Figure A5. Visibility (V_m) of scanner location pattern 13 in dependence of D_{dom} class and stem number class. D_{dom} class 1 ($D_{dom} \leq 20$), D_{dom} class 2 ($D_{dom} > 20$ and ≤ 40), D_{dom} class 3 ($D_{dom} > 40$ and ≤ 60), D_{dom} class 4 ($D_{dom} > 60$), N_{tree} class 1 ($N_{tree} \leq 100$), N_{tree} class 2 ($N_{tree} > 100$ and ≤ 500), N_{tree} class 3 ($N_{tree} > 500$ and ≤ 1000), N_{tree} class 4 ($N_{tree} > 1000$).

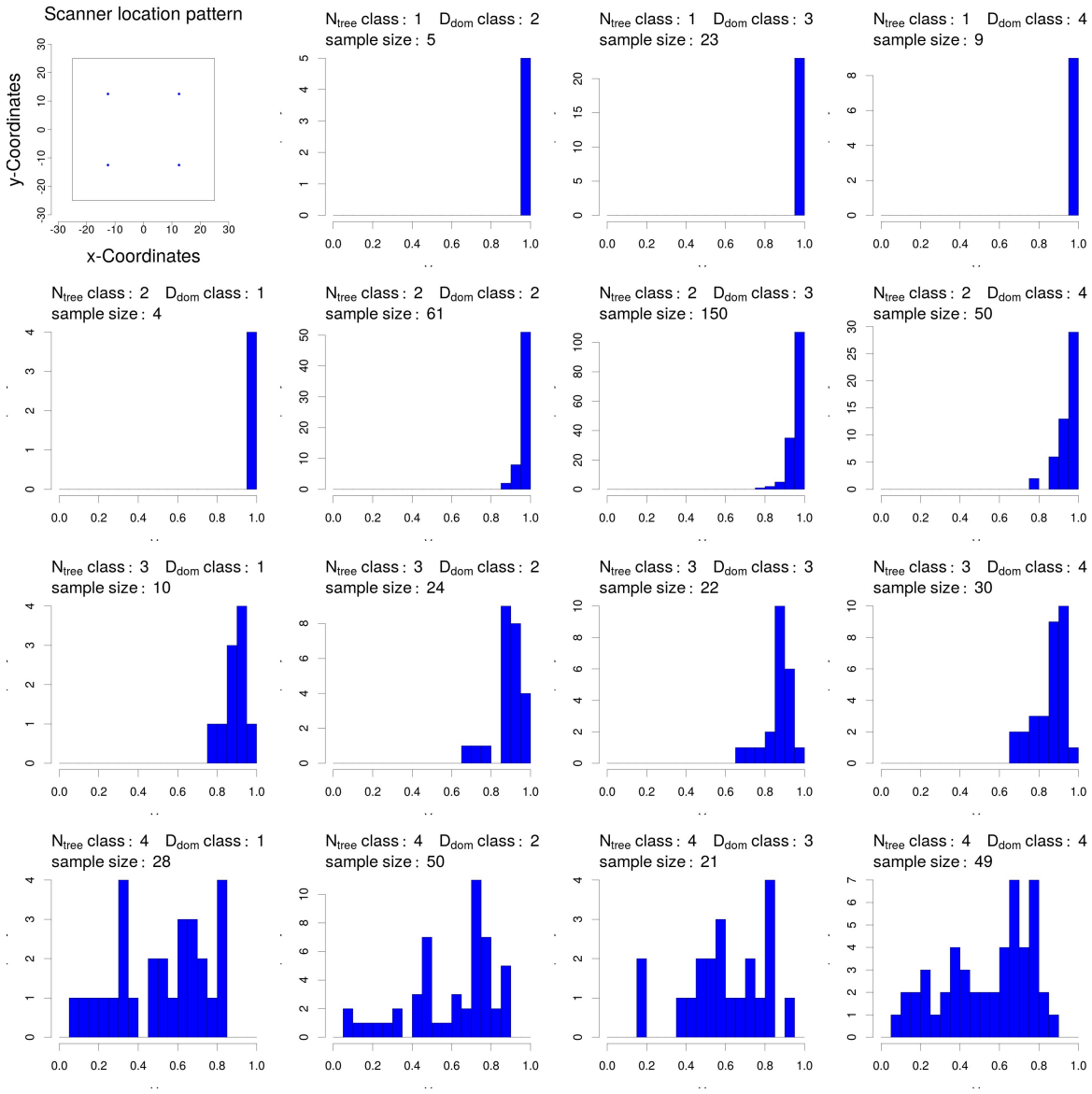

Figure A6. Visibility (V_m) of scanner location pattern 24 in dependence of D_{dom} class and stem number class. D_{dom} class 1 ($D_{dom} \leq 20$), D_{dom} class 2 ($D_{dom} > 20$ and ≤ 40), D_{dom} class 3 ($D_{dom} > 40$ and ≤ 60), D_{dom} class 4 ($D_{dom} > 60$), N_{tree} class 1 ($N_{tree} \leq 100$), N_{tree} class 2 ($N_{tree} > 100$ and ≤ 500), N_{tree} class 3 ($N_{tree} > 500$ and ≤ 1000), N_{tree} class 4 ($N_{tree} > 1000$).

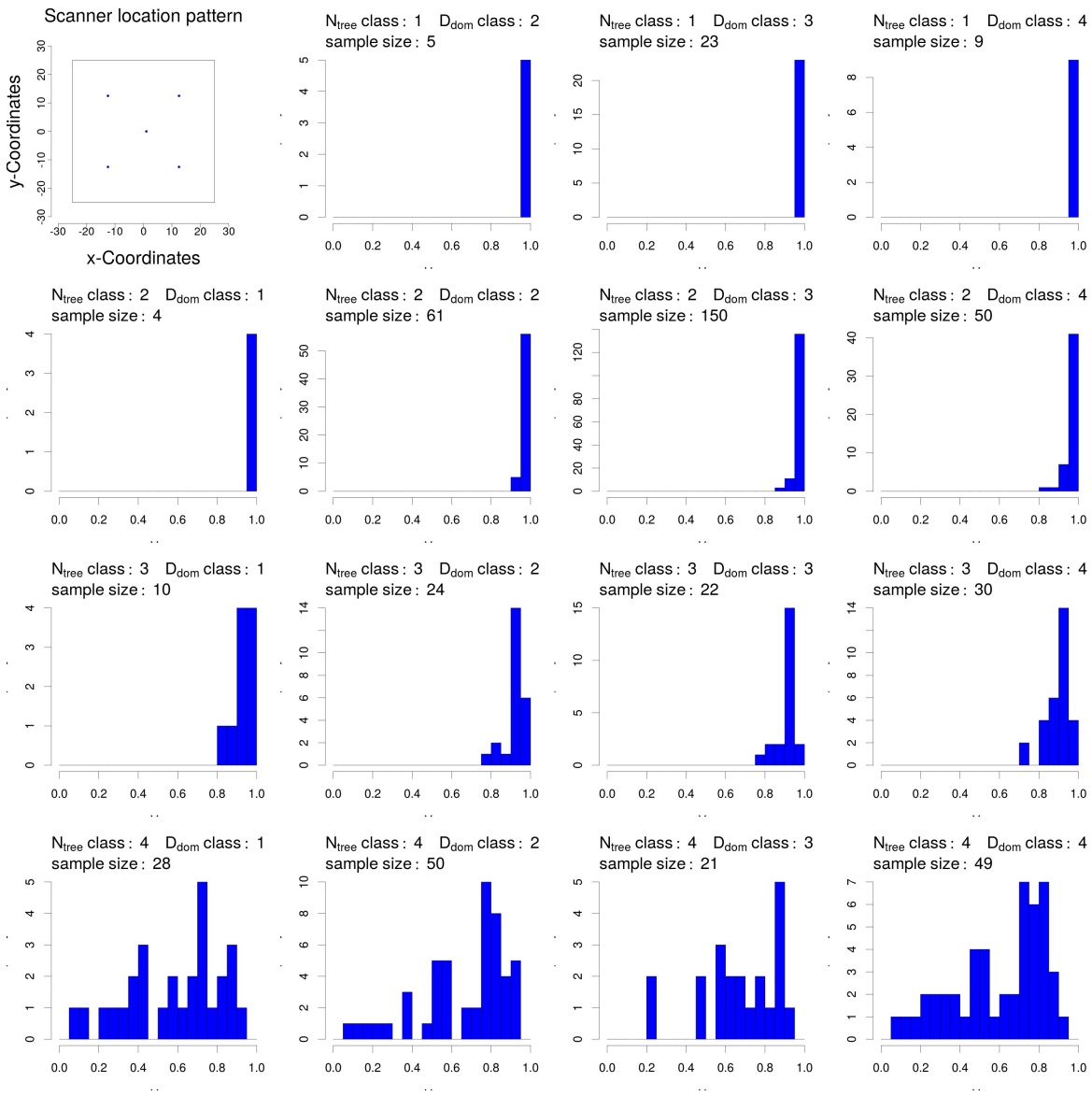

Figure A7. Visibility (V_m) of scanner location pattern 35 in dependence of D_{dom} class and stem number class. D_{dom} class 1 ($D_{dom} \leq 20$), D_{dom} class 2 ($D_{dom} > 20$ and ≤ 40), D_{dom} class 3 ($D_{dom} > 40$ and ≤ 60), D_{dom} class 4 ($D_{dom} > 60$), N_{tree} class 1 ($N_{tree} \leq 100$), N_{tree} class 2 ($N_{tree} > 100$ and ≤ 500), N_{tree} class 3 ($N_{tree} > 500$ and ≤ 1000), N_{tree} class 4 ($N_{tree} > 1000$).

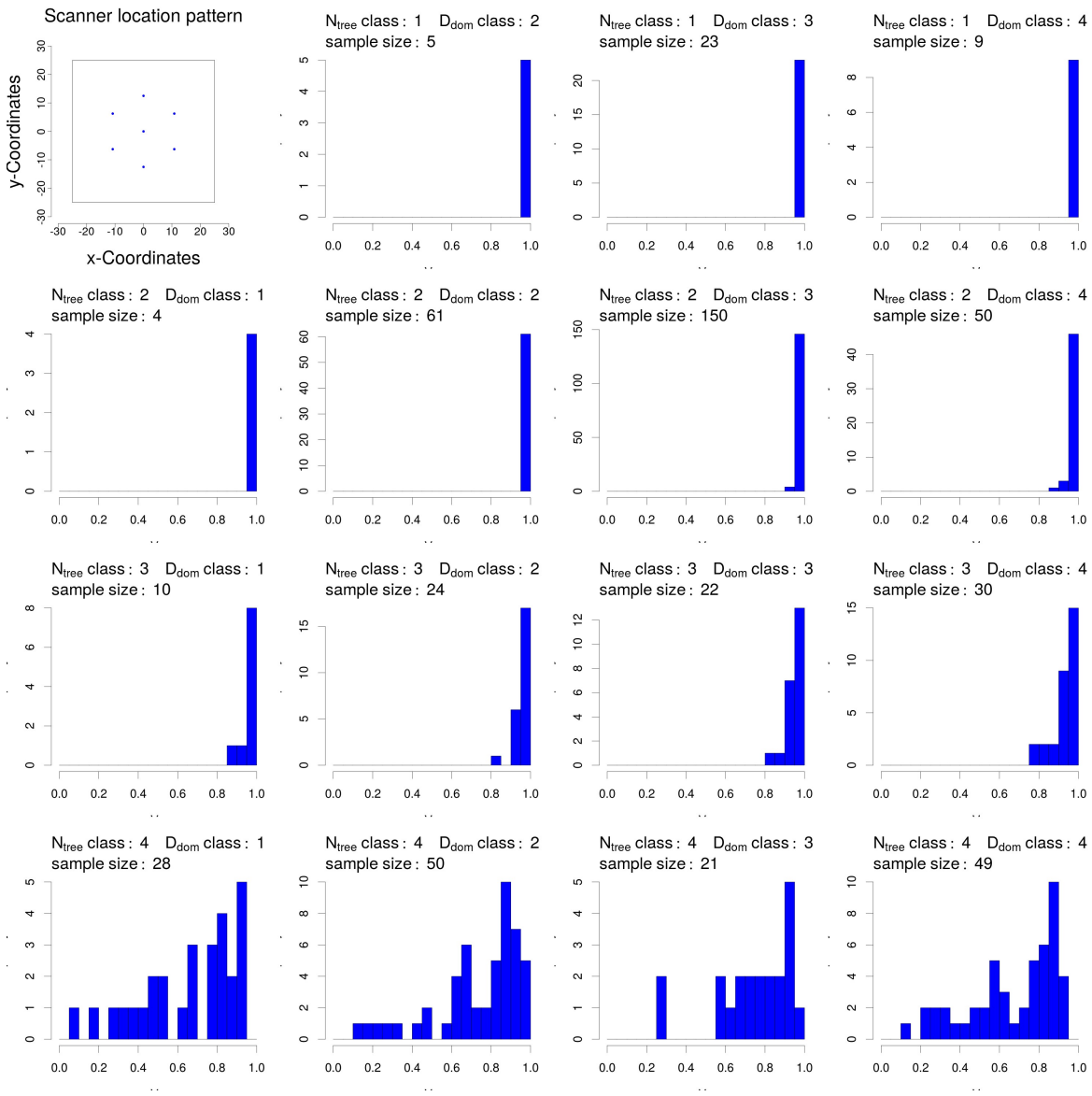

Figure A8. Visibility (V_m) of scanner location pattern 36 in dependence of D_{dom} class and stem number class. D_{dom} class 1 ($D_{dom} \leq 20$), D_{dom} class 2 ($D_{dom} > 20$ and ≤ 40), D_{dom} class 3 ($D_{dom} > 40$ and ≤ 60), D_{dom} class 4 ($D_{dom} > 60$), N_{tree} class 1 ($N_{tree} \leq 100$), N_{tree} class 2 ($N_{tree} > 100$ and ≤ 500), N_{tree} class 3 ($N_{tree} > 500$ and ≤ 1000), N_{tree} class 4 ($N_{tree} > 1000$).

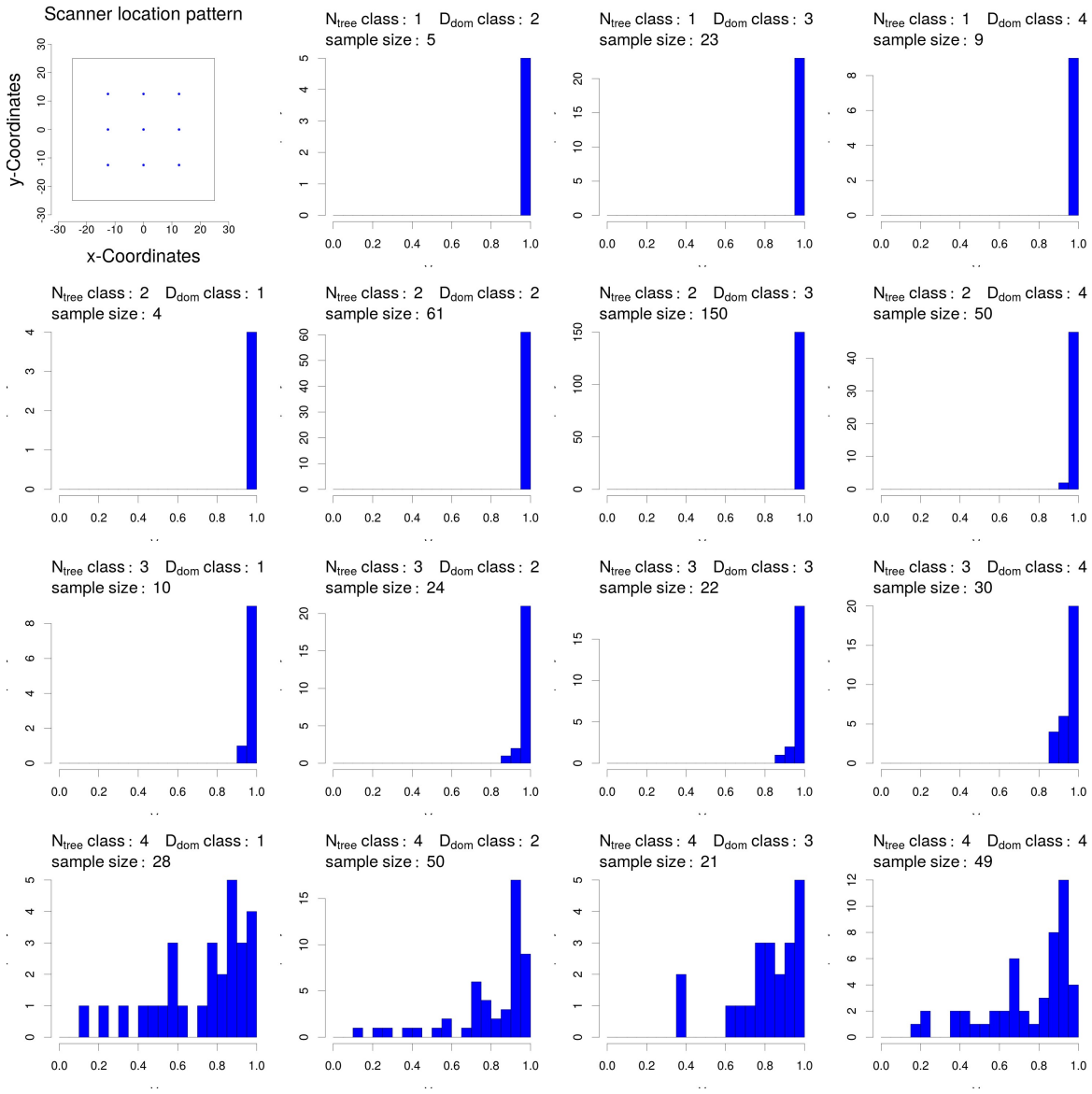

Figure A9. Visibility (V_m) of scanner location pattern 37 in dependence of D_{dom} class and stem number class. D_{dom} class 1 ($D_{dom} \leq 20$), D_{dom} class 2 ($D_{dom} > 20$ and ≤ 40), D_{dom} class 3 ($D_{dom} > 40$ and ≤ 60), D_{dom} class 4 ($D_{dom} > 60$), N_{tree} class 1 ($N_{tree} \leq 100$), N_{tree} class 2 ($N_{tree} > 100$ and ≤ 500), N_{tree} class 3 ($N_{tree} > 500$ and ≤ 1000), N_{tree} class 4 ($N_{tree} > 1000$).

References

1. FOREST EUROPE. *State of Europe's Forests 2015*; Ministerial Conference on the Protection of Forests in Europe: Madrid, Spain, 2015. Available online: http://enb.iisd.org/forestry/europe/mc/2015/ (accessed on 26 May 2017).
2. MacDicken, K.; Jonsson, Ö.; Piña, L.; Marklund, L.; Maulo, S.; Contessa, V.; Adikari, Y.; Garzuglia, M.; Lindquist, E.; Reams, G.; et al. *Global Forest Resources Assessment 2015: How Are the World's Forests Changing?* Food and Agriculture Organistation of the United Nations (FAO): Roma, Italy, 2016.
3. Pan, Y.; Birdsey, R.A.; Fang, J.; Houghton, R.; Kauppi, P.E.; Kurz, W.A.; Phillips, O.L.; Shvidenko, A.; Lewis, S.L.; Canadell, J.G.; et al. A Large and Persistent Carbon Sink in the World's Forests. *Science* **2011**, *333*, 988–993.
4. Shvidenko, A.; Barber, C.V.; Persson, R. *Forest and Woodland Systems*; Island Press: Washington, DC, USA, 2005; Chapter 21, pp. 585–621.

5. Brassel, P.; Lischke, H. *Swiss National Forest Inventory: Methods and Models of the Second Assessment*; WSL Swiss Federal Research Institute: Birmensdorf, Switzerland, 2001.
6. Tomppo, E.; Gschwantner, T.; Lawrence, M.; McRoberts, R.E. *National Forest Inventories*; Springer: Berlin, Germany, 2010.
7. Lovell, J.; Jupp, D.; Newnham, G.; Coops, N.; Culvenor, D. Simulation study for finding optimal lidar acquisition parameters for forest height retrieval. *For. Ecol. Manag.* **2005**, *214*, 398–412.
8. Disney, M.; Lewis, P.; Raumonen, P. Testing a new vegetation structure retrieval algorithm from terrestrial lidar scanner data using 3D models. In Proceedings of the Silvilaser 2012, Vancouver, BC, Canada, 16–18 September 2012.
9. Van der Zande, D.; Jonckheere, I.; Stuckens, J.; Verstraeten, W.W.; Coppin, P. Sampling design of ground-based lidar measurements of forest canopy structure and its effect on shadowing. *Can. J. Remote Sens.* **2008**, *34*, 526–538.
10. Binney, J.; Sukhatme, G.S. 3D tree reconstruction from laser range data. In Proceedings of the ICRA'09 IEEE International Conference on Robotics and Automation, Kobe, Japan, 12–17 May 2009.
11. Watt, P.J.; Donoghue, D.N.M. Measuring forest structure with terrestrial laser scanning. *Int. J. Remote Sens.* **2005**, *26*, 1437–1446.
12. Trochta, J.; Kral, K.; Janik, D.; Adam, D. Arrangement of terrestrial laser scanner positions for area-wide stem mapping of natural forests. *Can. J. For. Res.* **2013**, *43*, 355–363.
13. Van der Zande, D.; Hoet, W.; Jonckheere, I.; van Aardt, J.; Coppin, P. Influence of measurement set-up of ground-based LiDAR for derivation of tree structure. *Agric. For. Meteorol.* **2006**, *141*, 147–160.
14. Hilker, T.; Coops, N.C.; Culvenor, D.S.; Newham, G.; Wulder, M.A.; Bater, C.W.; Siggins, A. A simple technique for co-registration of terrestrial LiDAR observations for forestry applications. *Remote Sens. Lett.* **2012**, *3*, 239–247.
15. Wezyk, P.; Koziol, K.; Glista, M.; Pierzchalski, M. Terrestrial Laser Scanning versus Traditional Forest Inventory. First Result from the Polish Forests. ISPRS Workshop on Laser Scanning 2007 and SilviLaser 2007. In Proceedings of the International Archives of the Photogrammetry, Remote Sensing and Spatial Information Sciences, Espoo, Finland, 12–14 September 2007; Volume XXXVI-3/W52, pp. 424–429.
16. Yang, X.; Strahler, A.H.; Schaaf, C.B.; Jupp, D.L.B.; Yao, T.; Zhao, F.; Wang, Z.; Culvenor, D.S.; Newnham, G.J.; Lovell, J.; et al. Three-dimensional forest reconstruction and structural parameter retrievals using a terrestrial full-waveform lidar instrument (Echidna). *Remote Sens. Environ.* **2013**, *135*, 36–51.
17. Liang, X.; Kankare, V.; Hyyppä, J.; Wang, Y.; Kukko, A.; Haggrén, H.; Yu, X.; Kaartinen, H.; Jaakkola, A.; Guan, F.; et al. Terrestrial laser scanning in forest inventories. *ISPRS J. Photogramm. Remote Sens.* **2016**, *115*, 63–77.
18. Keller, M. *Swiss National Forest Inventory. Manual of the Field Survey 2004–2007*; Swiss Federal Research Institute WSL: Birmensdorf, Switzerland, 2011.
19. Mandallaz, D. *Sampling Techniques for Forest Inventories*; Chapman & Hall/CRC Applied Environmental Statistics; Chapman and Hall/CRC: Boca Raton, FL, USA, 2006.
20. Bailey, R.L.; Dell, T.R. Quantifying diameter distributions with the Weibull function. *For. Sci.* **1973**, *19*, 97–104.
21. Blender Online Community. *Blender—A 3D Modelling and Rendering Package*; Blender Foundation, Blender Institute: Amsterdam, The Netherlands, 2015.
22. Gschwandtner, M.; Kwitt, R.; Uhl, A.; Pre, W. BlenSor: Blender Sensor Simulation Toolbox. In *Advances in Visual Computing, Proceedings of the 7th International Symposium (ISVC 2011), Las Vegas, NV, USA, 26–28 September 2011*; Bebis, G., Boyle, R., Parvin, B., Koracin, D., Chung, R., Hammoud, R., Eds.; Springer: Berlin, Germany, 2011; Volume 6939/2011, pp. 199–208.
23. Kükenbrink, D.; Schneider, F.D.; Leiterer, R.; Schaepman, M.E.; Morsdorf, F. Quantificationof hidden canopy volume of airborne laser scanning data using a voxel traversal algorithm. *Remote Sens. Environ.* **2017**, *194*, 424–436.
24. Amanatides, J.; Woo, A. A Fast Voxel Traversal Algorithm for Ray Tracing. In Proceedings of the Eurographics 87, Amsterdam, The Netherlands, 24–28 August 1987; pp. 3–10.
25. Fisher, P.F. First Experiments in Viewshed Uncertainty: The Accuracy of the Viewshed Area. *Photogramm. Eng. Remote Sens.* **1991**, *57*, 1321–1327.

26. Travis, M.R.; Elsner, G.H.; Iverson, W.D.; Johnson, C.G. *VIEWIT: Computation of Seen Areas, Slope, and Aspect for Land-Use Planning*; Technical Report; Pacific Southwest Research Station; Forest Service; U.S. Department of Agriculture: Berkeley, CA, USA, 1975.
27. Gaulton, R.; Danson, F.; Ramirez, F.; Gunawan, O. The potential of dual-wavelength laser scanning for estimating vegetation moisture content. *Remote Sens. Environ.* **2013**, *132*, 32–39.
28. R Core Team. *R: A Language and Environment for Statistical Computing*; R Foundation for Statistical Computing: Vienna, Austria, 2017.
29. Mosteller, F.; Tukey, J.W. *Data Analysis and Regression: A Second Course in Statistics*; Addison-Wesley: Boston, MA, USA, 1977.
30. Antonarakis, A.S. Evaluating forest biometrics obtained from ground lidar in complex riparian forests. *Remote Sens. Lett.* **2011**, *2*, 61–70.
31. Liang, X.; Hyyppä, J. Automatic Stem Mapping by Merging Several Terrestrial Laser Scans at the Feature and Decision Levels. *Sensors* **2013**, *13*, 1614–1634.
32. Liang, X.; Kankare, V.; Yu, X.; Hyyppä, J.; Holopainen, M. Automated Stem Curve Measurement Using Terrestrial Laser Scanning. *IEEE Trans. Geosci. Remote Sens.* **2014**, *52*, 1739–1748.
33. Thies, M.; Pfeifer, N.; Winterhalder, D.; Gorte, B. Three-dimensional reconstruction of stems for assessment of taper, sweep and lean based on laser scanning of standing trees. *Scand. J. For. Res.* **2006**, *19*, 571–581.
34. Bienert, A.; Scheller, S.; Keane, E.; Mullooly, G.; Mohan, F. Application of terrestrial laser scanners for the determination of forest inventory parameters. Commission V Symposium 'Image Engineering and Vision Metrology'. In Proceedings of the International Archives of the Photogrammetry, Remote Sensing and Spatial Information Sciences, Dresden, Germany, 25–27 September 2006; Volume XXXVI, part 5, p. 5.
35. Maas, H.G.; Bienert, A.; Scheller, S.; Keane, E. Automatic forest inventory parameter determination from terrestrial laser scanner data. *Int. J. Remote Sens.* **2008**, *29*, 1579–1593.
36. Côté, J.F.; Fournier, R.A.; Frazer, G.W.; Niemann, K.O. A fine-scale architectural model of trees to enhance LiDAR-derived measurements of forest canopy structure. *Agric. For. Meteorol.* **2012**, *166–167*, 72–85.
37. Simonse, M.; Aschoff, T.; Spiecker, H.; Thies, M. Automatic Determination of Forest Inventory Parameters using Terrestrial Laser Scanning. In Proceedings of the ScandLaser Scientific Workshop on Airborne Laser Scanning of Forests, Umeå, Sweden, 3–4 September 2003; pp. 251–257.
38. Eysn, L.; Pfeifer, N.; Ressl, C.; Hollaus, M.; Grafl, A.; Morsdorf, F. A Practical Approach for Extracting Tree Models in Forest Environments Based on Equirectangular Projections of Terrestrial Laser Scans. *Remote Sens.* **2013**, *5*, 5424–5448.
39. Yao, T.; Yang, X.; Zhao, F.; Wang, Z.; Zhang, Q.; Jupp, D.; Lovell, J.; Culvenor, D.; Newnham, G.; Ni-Meister, W.; et al. Measuring forest structure and biomass in New England forest stands using Echidna ground-based lidar. *Remote Sens. Environ.* **2011**, *115*, 2965–2974.
40. Calders, K.; Newnham, G.; Burt, A.; Murphy, S.; Raumonen, P.; Herold, M.; Culvenor, D.; Avitabile, V.; Disney, M.; Armston, J.; et al. Nondestructive estimates of above-ground biomass using terrestrial laser scanning. *Methods Ecol. Evol.* **2015**, *6*, 198–208.
41. Woodgate, W.; Armston, J.D.; Disney, M.; Jones, S.D.; Suarez, L.; Hill, M.J.; Wilkes, P.; Soto-Berelov, M. Quantifying the impact of woody material on leaf area index estimation from hemispherical photography using 3D canopy simulations. *Agric. For. Meteorol.* **2016**, *226–227*, 1–12.
42. Newnham, G.J.; Armston, J.D.; Calders, K.; Disney, M.I.; Lovell, J.L.; Schaaf, C.B.; Strahler, A.H.; Danson, F.M. Terrestrial Laser Scanning for Plot-Scale Forest Measurement. *Curr. For. Rep.* **2015**, *1*, 239–251.
43. Dassot, M.; Constant, T.; Fournier, M. The use of terrestrial LiDAR technology in forest science: Application fields, benefits and challenges. *Ann. For. Sci.* **2011**, *68*, 959–974.
44. Raumonen, P.; Kaasalainen, M.; Akerblom, M.; Kaasalainen, S.; Kaartinen, H.; Vastaranta, M.; Holopainen, M.; Disney, M.; Lewis, P. Fast automatic Precision Tree Models from Terrestrial Laser Scanner Data. *Remote Sens.* **2013**, *5*, 491–520.
45. Hackenberg, J.; Morhart, C.; Sheppard, J.; Spiecker, H.; Disney, M. Highly Accurate Tree Models Derived from Terrestrial Laser Scan Data: A Method Description. *Forests* **2014**, *5*, 1069–1105.
46. Stoyan, D.; Stoyan, H. Non-Homogeneous Gibbs Process Models for Forestry—A Case Study. *Biom. J.* **1998**, *40*, 521–531.

47. Law, R.; Illian, J.; Burslem, D.F.R.P.; Gratzer, G.; Gunatilleke, C.V.S.; Gunatilleke, I.A.U.N. Ecological information from spatial patterns of plants: Insights from point process theory. *J. Ecol.* **2009**, *97*, 616–628.
48. Penttinen, A.; Stoyan, D.; Henttonen, H.M. Marked Point PrProcess in Forest Statistics. *For. Sci.* **1992**, *38*, 806–824.
49. Hopkinson, C.; Chasmer, L.; Young-Pow, C.; Treitz, P. Assessing forest metrics with a ground-based scanning lidar. *Can. J. For. Res.* **2004**, *34*, 573–583.
50. Kelbe, D.; Romanczyk, P.; van Aardt, J.; Cawse-Nicholson, K.; Krause, K. Automatic extraction of tree stem models from single rerrestrial lidar scans in structurally heterogeneous forest environments. In Proceedings of the Silvilaser 2012, Vancouver, BC, Canada, 16–18 September 2012.
51. Abegg, M.; Brändli, U.B.; Cioldi, F.; Fischer, C.; Herold-Bonardi, A.; Huber, M.; Keller, M.; Meile, R.; Rösler, E.; Speich, S.; et al. Viertes Schweizerisches Landesforstinventar–Ergebnistabellen und Karten im Internet zum LFI 2009–2013 (LFI4b). 2014. Available online: https://doi.org/10.21258/1000001 (accessed on 25 May 2017).

© 2017 by the authors. Licensee MDPI, Basel, Switzerland. This article is an open access article distributed under the terms and conditions of the Creative Commons Attribution (CC BY) license (http://creativecommons.org/licenses/by/4.0/).